Vacancy-model interpretation of EPR spectrum of Si:Pt$^-$

Frederick G. Anderson, Frank S. Ham, and George D. Watkins
Department of Physics and Sherman Fairchild Laboratory, Lehigh University, Bethlehem, Pennsylvania 18015
(Received 10 June 1991)

The vacancy model for platinum in silicon as proposed by Watkins postulates a neutral Pt atom in the $5d^{10}$ electronic configuration occupying a negatively charged lattice vacancy, so that electronic properties of Pt$^-$ should be similar to those of the isolated vacancy V^-. We show that this model, including strong Pt spin-orbit coupling and a Jahn-Teller (JT) distortion of C_{2v} symmetry combining tetragonal and trigonal components, and having only $\sim 10\%$ of the electronic wave function localized on the Pt, is qualitatively consistent with the results of the electron-paramagnetic-resonance (EPR) studies of Woodbury and Ludwig, which revealed an unusual form for the g tensor (nearly axial about $\langle 100 \rangle$ but departing strongly from the spin-only value of 2, with $g_\perp < 2 < g_\parallel$). The model accounts also for the anisotropic Pt hyperfine interaction and for superhyperfine interaction found to involve only two of the four nearest-neighbor Si atoms. With three electrons in t_2 vacancylike orbitals the JT distortion has two energetically similar forms yielding the same C_{2v} symmetry, one of which occurs for V^- and the other for Pt$^-$. With this identification, opposite signs found for the experimental strain-coupling coefficients of V^- and Pt$^-$ may be explained. The vacancy model predicts a positive value for the product $g_{xx}g_{yy}g_{zz}$, the opposite of that given by an alternative model due to Ammerlaan and van Oosten, which predicts $\sim 70\%$ localization in the Pt $5d$ shell. These models can, therefore, be distinguished by an experiment that determines this sign.

I. INTRODUCTION

Observation of the electron paramagnetic resonance (EPR) of platinum in silicon was reported by Woodbury and Ludwig[1] in 1962. The predominant spectrum found at low temperatures ($T < 12$ K) is anisotropic, corresponding to a defect of orthorhombic (C_{2v}) symmetry, and was interpreted by Woodbury and Ludwig as resulting from a single substitutional platinum in the charge state Pt$^-$ with spin $S = \frac{1}{2}$, at a site distorted by displacement of the Pt ion along a $\langle 100 \rangle$ direction. Later EPR studies[2-5] have confirmed these observations, despite a claim by Henning and Egelmeers[2] suggesting evidence of hyperfine coupling with a second nearby Pt atom. Henning and Egelmeers[2] also reported that analysis of strain-induced shifts in the g tensor as determined by a strain-modulated EPR detection technique indicated a lower symmetry compatible with such a Pt-Pt pair. Milligan, Anderson, and Watkins[3] have shown, however, that studies of the hyperfine coupling of samples enriched in the isotope ^{195}Pt or ^{198}Pt do not support the proposal for the presence of a second Pt, and in a companion paper[6] (paper I) to the present one these authors report direct studies of stress-induced g shifts that show the defect symmetry to be C_{2v}, supporting the model of an isolated Pt$^-$.

Despite the now widespread concurrence that this spectrum results from a single substitutional Pt$^-$ ion, there has been no corresponding agreement on a model for the defect's electronic configuration, despite the lapse of nearly 30 years since the work of Woodbury and Ludwig. Several possible such models were briefly discussed by Woodbury and Ludwig in their original paper[1] without going into detail. An early attempt at a detailed model to account for the anisotropy of the g tensor was made by Lowther,[7] who ascribed the resonance to a hole occupying a bonding molecular orbital outside a diamagnetic Pt $5d$ shell and proposed that the g tensor could be fitted if the hole were in an effective p state. An alternative proposed by Ammerlaan and van Oosten[8] places a hole predominantly in the $5d$ shell and shows that the g tensor can be matched to this model if the Pt is covalently bonded to two neighboring Si atoms.

Watkins[9] has proposed a "vacancy model" for Pt$^-$ in silicon to account for the spin ($S = \frac{1}{2}$) and for the defect's dihedral $\langle 100 \rangle$ distortion from the tetrahedral symmetry of a substitutional site. Starting from the results of the theoretical calculations by Cartling,[10] Hemstreet,[11] and Zunger and Lindefelt[12] on substitutional transition-metal impurities in silicon, which showed that near the end of each series the d levels lie deep in the valence band, Watkins postulated for Pt$^-$ a neutral Pt atom in the $5d^{10}$ configuration occupying a negatively charged lattice vacancy. The electronic properties of the isolated vacancy V^- are indeed similar to those of Pt$^-$, V^- also having $S = \frac{1}{2}$ and a dihedral $\langle 100 \rangle$ Jahn-Teller (JT) distortion.[13] The t_2 orbitals responsible for the resonance in the vacancy model are primarily located on the silicon neighbors, so that this model contrasts with the conclusion of Ammerlaan and van Oosten[8] that the hole is $\sim 70\%$ localized in the Pt $5d$ shell.

The purpose of the present paper is to develop the vacancy model in greater detail as a test of its applicability to Pt$^-$. We will be concerned particularly with the g tensor, which for Pt$^-$ shows large departures from the spin-only value 2.0023, and with hyperfine coupling to both the central Pt and the four nearest-neighbor Si atoms. The spectrum shows that significant hyperfine coupling occurs with only two of these neighbors, and it is clearly

a requirement of a successful model that it yield the correct pair while reproducing the anisotropies of both the g tensor and the Pt hyperfine tensor. We are especially concerned with showing how the vacancy model leads to static JT distortions of the form observed. As shown from the stress data of the accompanying paper,[6] these distortions (in both tetragonal and trigonal modes) have the opposite sense for Pt^- from that found for V^-, and we take as evidence strongly supporting the vacancy model that it can account very naturally for this difference. By contrast, the models of Lowther[7] and Ammerlaan and van Oosten,[8] though they can fit the anisotropy in the g tensor (though not that of the Pt hyperfine tensor), do not yield JT distortions of the correct form and thus do not account for the spontaneous nature of these distortions. We will explore these alternative models with some care in order to make clear their successes and weaknesses and to show exactly how they differ from the vacancy model, all these models being based on various degrees of occupancy of a t_2 manifold of states (effective p states) in the presence of spin-orbit coupling comparable in strength to the crystal-field splittings.

We will not attempt in this paper to achieve an exact numerical fit to the experimental data for the g and hyperfine tensors, because, as Anderson, Delerue, Lannoo, and Allan[14] show elsewhere in making such a fit to a phenomenological description of Pt^- based on the vacancy model, it is necessary in doing so to include other states (e.g., the remaining d orbitals of Pt) outside the t_2 manifold of vacancy orbitals. Including these additional states complicates the analysis beyond our purpose of presenting the general features of the vacancy model and showing that it is more successful than alternative models in describing the Pt^- center.

An outline of this paper is as follows. In Sec. II A we introduce the vacancy model and describe its alternative possible forms of JT distortion as illustrated by the Pt^- and V^- centers. Section II B shows how a strong spin-orbit interaction resulting from the presence of the central Pt atom leads to a g tensor that can depart strongly from the spin-only value and in a first approximation has axial symmetry about $\langle 100 \rangle$, even though the actual defect symmetry is orthorhombic (C_{2v}). The fact that this spin-orbit coupling is of comparable strength to the crystal-field splitting caused by the trigonal field makes it essential for us to distinguish clearly in Sec. II C between the true electron spin and the effective-spin operator used in forming the spin Hamiltonian that describes the response of each Kramers-doublet level to perturbations. Also in Sec. II C we make corrections needed to include nonaxial components of the g tensor. Sections II D and II E describe hyperfine coupling with the Pt and the nearest-neighbor Si, respectively. Section II F analyzes the effect of applied stress in shifting the relative energies of the six different orientations of the distorted center, and Sec. II G relates the corresponding strain-coupling coefficients to the tetragonal and trigonal JT energies. In Sec. III A we compare our theoretical expressions for the g factors and hyperfine parameters with those obtained from the experimental EPR data, and in Sec. III B we interpret the experimental strain-coupling coefficients in terms of the JT energies and relate them to the corresponding results for V^-. Section IV contrasts the vacancy model with the alternative models for Pt^- proposed by Lowther and by Ammerlaan and van Oosten. We discuss our results and conclusions in Sec. V. An Appendix gives the corresponding treatment of the spin Hamiltonian for a second Kramers-doublet level, which is doubly occupied in the vacancy model for Pt^- but is the magnetic level in the alternative models.

II. ELECTRONIC STRUCTURE

A. Vacancy model with Jahn-Teller coupling

In this section we describe the vacancy model for the electronic structure of the Pt^- defect in silicon, taking this defect to be an isolated, substitutional Pt impurity in its singly minus charge state. The suitability of Watkins's original proposal of the vacancy model for Pt^- was subsequently confirmed by cluster calculations by Alves and Leite[15] specifically for substitutional Pt^-. The basic idea of the model is illustrated in Fig. 1. The vacancy t_2 states that lie within the band gap in this model result from the dangling bonds on the silicon atoms surrounding the vacancy and interact weakly with the impurity d states of t_2 symmetry, which are deep in the valence band for transition-metal ions at the end of each series. Only a small amount of the impurity d states should be mixed into the vacancy t_2 states, therefore, and the resulting molecular orbitals should be vacancylike in character.

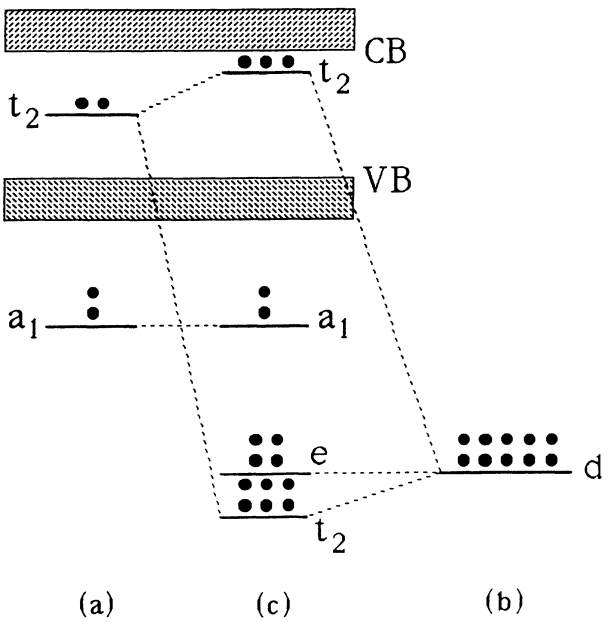

FIG. 1. One-electron energy levels of (a) the silicon vacancy in full tetrahedral symmetry, (b) the 5d states of the Pt atom, and (c) an isolated substitutional Pt impurity in silicon (with no JT distortion). The interaction of the t_2 component of the 5d states of the Pt atom with the t_2 gap states of the vacancy, leading for the Pt defect to deep bonding states and antibonding t_2 gap states, is indicated schematically. The indicated electronic occupancies of the levels correspond to (a) the neutral vacancy, (b) the neutral Pt atom, and (c) the Pt^- defect.

These orbitals can be written simply as

$$|i\rangle = N\phi_i^{\mathrm{Pt}} + M\phi_i^{\mathrm{vac}} , \tag{1}$$

where M and N are factors that determine the relative proportion of vacancylike and Pt components, and $i = \xi, \eta, \zeta$ denotes orbitals transforming in tetrahedral symmetry as $y'z'$, $z'x'$, and $x'y'$ (or x', y', z'), respectively, in terms of coordinates relative to cubic axes of the crystal.

The population of this t_2 gap manifold is determined by the number of impurity valence electrons and the charge state of the defect. The neutral Pt atom has ten valence electrons that fill the deep t_2 and e impurity-induced states in the valence band. The neutral silicon vacancy has two electrons in the t_2 gap manifold, the other two filling the a_1 state in the valence band that represents the symmetric combination of the four dangling bonds. The Pt$^-$ defect therefore has three electrons in the t_2 gap manifold, as shown in Fig. 1. We expect that the Pt$^-$ defect should therefore be very similar to the negative vacancy (V^-), and in fact the spin ($S = \frac{1}{2}$) and the symmetry (C_{2v}) are the same for these defects.

The C_{2v} symmetry of the V^- defect is the result of two static JT distortions.[13] The first is a tetragonal distortion, in which the silicon nearest neighbors are displaced by pairs. Our analysis will consider that orientation for the defect for which the tetragonal distortion Q_θ is aligned with the z' axis [i.e., $Q_\theta \sim (3z'^2 - r^2)$], so that the state $|\zeta\rangle$ is split from the doublet $|\xi\rangle, |\eta\rangle$. The second distortion is a shear ($Q_\zeta \sim x'y'$) in which the two atoms in one pair move apart and the two of the opposite pair move closer, splitting the doublet. With a substitutional impurity present, this second distortion can also involve the displacement of the impurity along the z' axis. We will refer to this second distortion imprecisely as a trigonal distortion.

While the vacancy model predicts that these two JT distortions simultaneously occur and thus yields the correct symmetry, the model does not predict the ordering of the one-electron states in the distorted configuration when there are three electrons in the t_2 gap manifold, a result that has been recognized independently by Lannoo.[16] We demonstrate this for a tetragonal distortion alone in Fig. 2, where we have drawn two possible ways in which a t_2 state could split. In Fig. 2(a) the singlet $|\zeta\rangle$ is the ground state (as in the case of the V^- defect, see Ref. 13), and in Fig. 2(b) the doublet $|\xi\rangle, |\eta\rangle$ is the ground state. In each case, when these states are populated with three electrons, the sum of the one-electron energies is the same, since for linear coupling to the tetragonal distortion the energy displacement of the singlet state is twice that of the doublet but in the opposite sense. Neither splitting is therefore favored. It is easy to show that including the trigonal distortion does not change this conclusion.

For the case of the Pt$^-$ defect, we take the splitting to be that shown in Fig. 2(b), since with this choice each of the elements of the piezospectroscopic tensor for the Pt$^-$ defect will be shown in Sec. III B to have the opposite sign to that for the V^- defect, as found experimentally.[6]

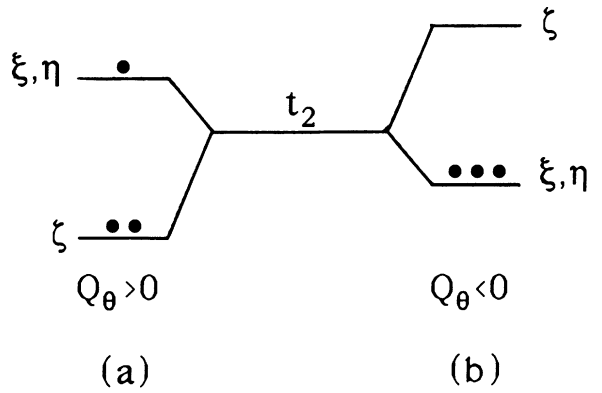

FIG. 2. Alternative ways in which a t_2 manifold of states may split via a tetragonal JT distortion. In (a) the singlet is the lower state, corresponding to one sense of the JT distortion mode ($Q_\theta > 0$, say), while in (b) the doublet is lower, corresponding to the opposite sense of the distortion. For three-electron occupancy as shown, with linear JT coupling to Q_θ, the sum of the one-electron energies is the same in (a) and in (b) for the same magnitude $|Q_\theta|$ of the distortion.

We assume, as with the V^- defect, that the splitting due to the tetragonal JT distortion is much larger than that due to the trigonal distortion.

Next we consider the JT coupling to the trigonal distribution, which splits the doublet. As a result of the two JT distortions, the t_2 gap manifold is therefore split into three states,

$$\begin{aligned}
|\zeta\rangle &= N\phi_\zeta^{\mathrm{Pt}} + (M/2)(\phi_a - \phi_b - \phi_c + \phi_d) , \\
|\alpha\rangle &= (|\xi\rangle + |\eta\rangle)/\sqrt{2} \\
&= (N/\sqrt{2})(\phi_\xi^{\mathrm{Pt}} + \phi_\eta^{\mathrm{Pt}}) + (M/\sqrt{2})(\phi_d - \phi_a) , \\
|\beta\rangle &= (-|\xi\rangle + |\eta\rangle)/\sqrt{2} \\
&= (N/\sqrt{2})(-\phi_\xi^{\mathrm{Pt}} + \phi_\eta^{\mathrm{Pt}}) + (M/\sqrt{2})(\phi_b - \phi_c) ,
\end{aligned} \tag{2}$$

where ϕ_a, ϕ_b, ϕ_c, and ϕ_d denote equivalent dangling bonds, directed toward the central Pt site, on nearest-neighbor silicon atoms lying in $[11\bar{1}]'$, $[1\bar{1}1]'$, $[\bar{1}11]'$, and $[\bar{1}\,\bar{1}\,\bar{1}]'$ directions, respectively, as illustrated in Fig. 3. (We denote a direction or plane with reference to the x', y', z' coordinate system by placing a prime on the corresponding bracket.) The coupling responsible for this second JT distortion is described by

$$H_{\mathrm{trig}} = -V_T Q_\zeta (|\alpha\rangle\langle\alpha| - |\beta\rangle\langle\beta|) , \tag{3}$$

where Q_ζ is the distortion coordinate and V_T the trigonal JT coupling coefficient. The molecular orbital $|\alpha\rangle$ is illustrated in Fig. 4. It consists of dangling bonds on silicon atoms a and d in addition to the central Pt orbital and is even and odd, respectively, under reflection in the $(1\bar{1}0)'$ and $(110)'$ planes. The orbital $|\beta\rangle$ is identical in form but with the dangling bonds on the b and c neighbors and the role of these reflection planes reversed. In describing the defect we will use a coordinate system coinciding with its principal axes as defined by these

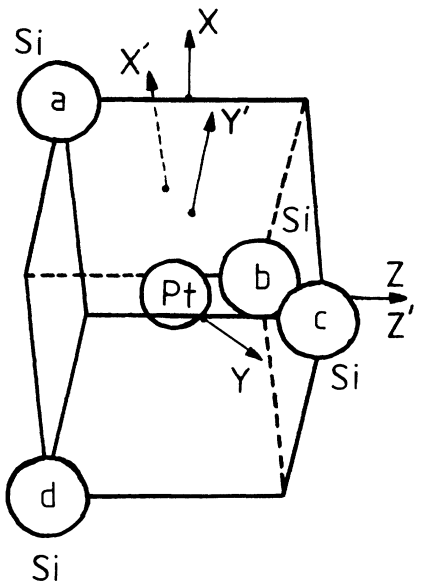

FIG. 3. Geometry of the undistorted substitutional site of a Pt impurity in silicon, showing the four nearest-neighbor Si sites a, b, c, and d. Coordinate axes (x',y',z') coinciding with cubic axes of the crystal are indicated by arrows. Also indicated are coordinate axes (x,y,z) in the principal axis system of a JT-distorted Pt^- defect oriented such that its tetragonal axis is along z': $x=(x'+y')/\sqrt{2}$, $y=(-x'+y')/\sqrt{2}$, $z=z'$.

reflection planes: $x=(x'+y')/\sqrt{2}$, $y=(-x'+y')/\sqrt{2}$, $z=z'$. These axes are also indicated in Fig. 3.

B. Role of spin-orbit interaction: Approximation of an axially symmetric g tensor

Spin-orbit interaction with respect to the one-electron t_2 orbitals of Eq. (1) in tetrahedral symmetry takes the simple form

$$H_{so}=\lambda(\mathcal{L}\cdot\mathbf{S}) , \tag{4}$$

where $\mathcal{L}$ is an effective orbital angular momentum operator defined[17] to have nonzero matrix elements only between these orbitals in every respect identical to those of true orbital angular momentum ℓ with respect to an atomic p state. Because of the large spin-orbit coupling $\zeta_{Pt}(\ell\cdot\mathbf{S})$ of the $5d$ states of atomic Pt, for which $\zeta_{Pt}=3368\ cm^{-1}$,[18] we may expect the principal contribution to the spin-orbit parameter λ of the defect to be that of the central Pt, given from Eq. (1) by

$$\lambda\cong -N^2\zeta_{Pt} , \tag{5}$$

if ϕ_i^{Pt} is approximated by a $5d$ atomic orbital. We note in particular that we expect to have $\lambda<0$.

The Zeeman interaction may be represented similarly by

$$H_Z=g_e\mu_B(\mathbf{S}\cdot\mathbf{B})+g_{\mathcal{L}}\mu_B(\mathcal{L}\cdot\mathbf{B}) , \tag{6}$$

with μ_B the Bohr magneton, and $g_e=2.0023$ and $g_{\mathcal{L}}$ are the spin and orbital g factors. In the approximation[19] of attributing orbital angular momentum only to the central Pt, as in Eq. (5), we have

$$g_{\mathcal{L}}\cong -N^2 . \tag{7}$$

We therefore expect to have $g_{\mathcal{L}}<0$, a consequence of $\mathcal{L}$ and ℓ having matrix elements of opposite sign but equal magnitude with respect to the t_2 components of atomic d orbitals.[17]

It is convenient to start our analysis with the exact spin-orbit state of the doublet $|\xi\rangle,|\eta\rangle$ in the configuration of the tetragonal JT distortion along the z axis, for which the symmetry is D_{2d}. The only term of H_{so} having matrix elements within this doublet is $\lambda\mathcal{L}_zS_z$, so that we have for the spin-orbit eigenstates one Kramers doublet

$$\begin{aligned} |A\rangle&=(|\alpha\rangle-i|\beta\rangle)/\sqrt{2} ,\\ |A^*\rangle&=(|\bar{\alpha}\rangle+i|\bar{\beta}\rangle)/\sqrt{2} , \end{aligned} \tag{8}$$

at energy $E=-\lambda/2$, where we use the basis $|\alpha\rangle$ and $|\beta\rangle$ defined by Eq. (2) and henceforth designate orbital states with $S_z=+\frac{1}{2}$ by $|\alpha\rangle,|\beta\rangle$ and those with $S_z=-\frac{1}{2}$ by $|\bar{\alpha}\rangle,|\bar{\beta}\rangle$, and a second doublet

$$\begin{aligned} |B\rangle&=(|\alpha\rangle+i|\beta\rangle)/\sqrt{2} ,\\ |B^*\rangle&=(|\bar{\alpha}\rangle-i|\bar{\beta}\rangle)/\sqrt{2} , \end{aligned} \tag{9}$$

at $E=\lambda/2$. Evaluating matrix elements of H_Z from Eq. (6), we find for a magnetic field $\mathbf{B}$ along the z axis that the Kramers doublet $|A\rangle$ and $|A^*\rangle$ splits as $\pm\frac{1}{2}g_{zz}\mu_BB$, corresponding to a g factor (effective spin $\frac{1}{2}$)

$$g_{zz}=g_e-2g_{\mathcal{L}} , \tag{10}$$

while for $|B\rangle$ and $|B^*\rangle$

$$g_z=g_e+2g_{\mathcal{L}} . \tag{11}$$

Both of these Kramers doublets do not split in magnetic fields perpendicular to the tetragonal axis and thus have $g_{xx}=g_{yy}=g_\perp=0$.

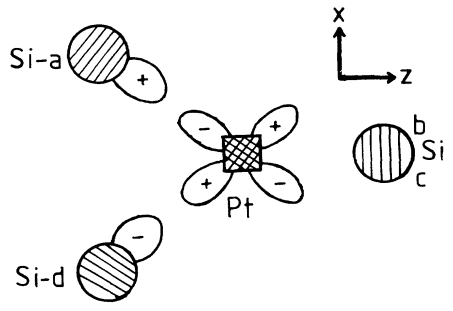

FIG. 4. Schematic representation of the molecular orbital $|\alpha\rangle$ defined in Eq. (2). The orbital is even and odd, respectively, under reflection in the xz and yz planes and comprises an antibonding combination of a Pt $5d$ orbital ($\sim xz$) with dangling bonds on the silicon atoms a and d.

Spin-orbit interaction couples the components $|\zeta\rangle, |\bar{\zeta}\rangle$ of the orbital singlet, which lies an energy Δ_ζ above the doublet $|\xi\rangle, |\eta\rangle$, with the Kramers doublet $|A\rangle, |A^*\rangle$, but not with $|B\rangle, |B^*\rangle$. Taking exact account of this coupling by H_{so} in Eq. (4), we must then replace $|A\rangle$ and $|A^*\rangle$ by

$$|A'\rangle = \cos\alpha |A\rangle - \sin\alpha |\bar{\zeta}\rangle ,$$
$$|A'^*\rangle = \cos\alpha |A^*\rangle + \sin\alpha |\zeta\rangle , \tag{12}$$

at energy $E = -(\lambda/2)(1+\sqrt{2}\tan\alpha)$, where α is given by

$$\tan 2\alpha = \lambda\sqrt{2}/(\Delta_\zeta + \tfrac{1}{2}\lambda) , \tag{13}$$

The trigonal JT coupling (3) mixes corresponding spin components of the two Kramers doublets (8) and (9). Treating exactly the resulting coupling between (A', A'^*) and (B, B^*) [but ignoring the weaker coupling to the states orthogonal to Eq. (12) in which $|\bar{\zeta}\rangle$ and $|\zeta\rangle$ predominate for $|\lambda/\Delta_\zeta| < 1$], we find one root at

$$E = -(\lambda/2)(1+\sqrt{2}\tan\alpha) - V_T Q_\zeta \cos\alpha \tan\theta , \tag{14}$$

corresponding to the Kramers doublet

$$|H\rangle = \cos\theta |A'\rangle + \sin\theta |B\rangle ,$$
$$|H^*\rangle = \cos\theta |A'^*\rangle + \sin\theta |B^*\rangle , \tag{15}$$

where θ is given by

$$\tan 2\theta = 2(V_T Q_\zeta/\lambda)\cos\alpha/(1+2^{-1/2}\tan\alpha) , \tag{16}$$

and a second root at

$$E = \tfrac{1}{2}\lambda + V_T Q_\zeta \cos\alpha \tan\theta , \tag{17}$$

corresponding to a doublet (L, L^*) given in the Appendix. In Eq. (16), θ is to be taken (for $\lambda < 0$) in the range $0 < \theta < \pi/4$ for $V_T Q_\zeta < 0$ and in the range $-\pi/4 < \theta < 0$ for $V_T Q_\zeta > 0$.

For both Kramers doublets (H, H^*) and (L, L^*) we find as a result of the mixing of the states of Eqs. (8) and (9) by H_{trig} that the perpendicular components of the g tensor are no longer zero. Ignoring in a first approximation the spin-orbit mixing with $|\zeta\rangle, |\bar{\zeta}\rangle$ (i.e., taking $\cos\alpha = 1$), we find that the symmetry of both g tensors remains axial, with

$$g_{zz} = g_\parallel = g_e - 2g_{\mathcal{L}}\cos 2\theta ,$$
$$g_\perp = g_e \sin 2\theta , \tag{18}$$

for the upper doublet (H, H^*). The departure of g_{zz} from g_e is caused by the orbital magnetic moment, but that of $g_\perp$ is the result of the spin-orbit coupling in mixing the states $|\alpha\rangle$ and $|\beta\rangle$ and thus reducing the matrix elements of the spin magnetic moment. For Pt$^-$, for which we expect to have $g_{\mathcal{L}} < 0$, we should therefore find $g_{zz} > g_e$ and the g tensor approximately axial with $0 < |g_\perp| < g_e$ if the unpaired electron is in the upper doublet (H, H^*) as expected for the t_2^3 electronic configuration of Fig. 2(b).

C. Effective spin: Nonaxial correction to the g tensor

In introducing the g factors in Eqs. (10), (11), and (18), we have implicitly made use of the concept of a spin Hamiltonian in terms of an effective spin $\frac{1}{2}$, the conventional practice[20] in describing the splitting of a Kramers doublet in magnetic fields or by hyperfine coupling. Ordinarily, the relation of effective spin to the true electron spin is self-evident, and there is no need to make it explicit. But for the states of the Pt$^-$ defect we have found that this relation can be ambiguous. It is important, therefore, to be clear in distinguishing effective spin from true spin, the relative signs of the g factors and hyperfine parameters being dependent on what choice is made in defining the effective spin.

In C_{2v} symmetry, a Kramers doublet such as (H, H^*) in Eq. (15) belongs to the irreducible representation Γ_5 of the double group,[21] while the true spin components S_x, S_y, and S_z (or the effective orbital angular momentum components $\mathcal{L}_x$, $\mathcal{L}_y$, and $\mathcal{L}_z$) transform, respectively, as the distinct representations Γ_4, Γ_2, and Γ_3. Because the direct product $\Gamma_5 \times \Gamma_5$ contains each of Γ_2, Γ_3, and Γ_4 only once, the Wigner-Eckart theorem assures us that all matrix elements of S_x with respect to $|H\rangle$ and $|H^*\rangle$ differ from those of any other operator transforming as Γ_4 by only a common proportionality factor. The same is true for S_y or S_z and any other operator transforming as Γ_2 or Γ_3 (with a differential proportionality factor in each case). In particular, in this symmetry we can define effective-spin operators $\mathcal{S}_x$, $\mathcal{S}_y$, and $\mathcal{S}_z$ that transforms as Γ_4, Γ_2, and Γ_3, respectively, and have matrix elements

$$\langle H|\mathcal{S}_x|H^*\rangle = \langle H^*|\mathcal{S}_x|H\rangle = \tfrac{1}{2} ,$$
$$\langle H|\mathcal{S}_y|H^*\rangle = -\langle H^*|\mathcal{S}_y|H\rangle = -i/2 , \tag{19}$$
$$\langle H|\mathcal{S}_z|H\rangle = -\langle H^*|\mathcal{S}_z|H^*\rangle = \tfrac{1}{2} ,$$

so that $\mathcal{S}_x$, $\mathcal{S}_y$, or $\mathcal{S}_z$ in the basis $|H\rangle, |H^*\rangle$ equals one-half the corresponding Pauli matrix, and the effective spin satisfies the commutation rules for spin $\frac{1}{2}$. Consistent with the Wigner-Eckart theorem, we then have

$$\langle H_i|S_x|H_j\rangle = (2uv - w^2)\langle H_i|\mathcal{S}_x|H_j\rangle ,$$
$$\langle H_i|S_y|H_j\rangle = (2uv + w^2)\langle H_i|\mathcal{S}_y|H_j\rangle , \tag{20}$$
$$\langle H_i|S_z|H_j\rangle = (1-2w^2)\langle H_i|\mathcal{S}_z|H_j\rangle ,$$

where (H_i, H_j) represents any combination from the pair of states (H, H^*), and we have represented $|H\rangle$ and $|H^*\rangle$ in an exact form consistent with Eqs. (8), (9), (12), and (15) (neglecting coupling to all states outside the t_2 gap manifold):

$$|H\rangle = u(|\alpha\rangle - i|\beta\rangle)/\sqrt{2} + v(|\alpha\rangle + i|\beta\rangle)/\sqrt{2} + w|\bar{\zeta}\rangle ,$$
$$|H^*\rangle = u(|\bar{\alpha}\rangle + i|\bar{\beta}\rangle)/\sqrt{2} + v(|\bar{\alpha}\rangle - i|\bar{\beta}\rangle)/\sqrt{2} - w|\zeta\rangle . \tag{21}$$

The coefficients u, v, and w are real, satisfying the normalization condition

$$u^2+v^2+w^2=1 , \tag{22}$$

and should be given to an excellent approximation, according to Eqs. (12) and (15), by

$$\begin{aligned} u &= \cos\theta\cos\alpha , \\ v &= \sin\theta , \\ w &= -\cos\theta\sin\alpha , \end{aligned} \tag{23}$$

with α and θ given by Eqs. (13) and (16).

The choice in defining the effective spin in Eq. (19) is a purely arbitrary one, but it is convenient in the case of the Pt^- defect, as we shall see, in causing g_{xx} and g_{yy} to have the same sign. If alternatively we had chosen to interchange $|H\rangle$ and $|H^*\rangle$ in assigning the $+\frac{1}{2}$ and $-\frac{1}{2}$ states of $\mathcal{S}_z$ and correspondingly had changed the signs of the matrix elements used to define $\mathcal{S}_y$ in order to preserve the spin-$\frac{1}{2}$ commutation rules, as done in the treatment of a similar problem by Bleaney and O'Brien,[22] we would have reversed the signs of the factors for S_y and S_z in Eq. (20) and correspondingly the spins of g_{yy} and g_{zz}. This choice would be a natural one, as motivated by the sense of the true spin in the components $|\bar{\xi}\rangle$ and $|\zeta\rangle$ in $|H\rangle$ and $|H^*\rangle$, respectively, in Eq. (21), if we had $|w| \gg |u|, |v|$. Other alternative choices for the definition of the effective spin, of course, would be equally valid, but in the present work we will use always that given by Eq. (19) [and for the state (L,L^*) of the Appendix the choice obtained from Eq. (19) by replacing H and H^* by L and L^*, respectively].

The spin Hamiltonian for the Zeeman splitting of either of the doublets (H,H^*) or (L,L^*) in C_{2v} symmetry must have the general form

$$\mathcal{H}_Z=\mu_B(g_{xx}\mathcal{S}_xB_x+g_{yy}\mathcal{S}_yB_y+g_{zz}\mathcal{S}_zB_z) , \tag{24}$$

since B_x, B_y, and B_z, like $\mathcal{S}_x$, $\mathcal{S}_y$, and $\mathcal{S}_z$, transform as Γ_4, Γ_2, and Γ_3, respectively. The g tensor for (H,H^*) is accordingly given exactly from Eq. (6), the spin matrix elements of Eq. (20), and the corresponding matrix elements of $\mathcal{L}_x$, $\mathcal{L}_y$, and $\mathcal{L}_z$ by

$$\begin{aligned} g_{xx} &= g_e(2uv-w^2)-g_{\mathcal{L}}2\sqrt{2}w(u-v) , \\ g_{yy} &= g_e(2uv+w^2)+g_{\mathcal{L}}2\sqrt{2}w(u+v) , \\ g_{zz} &= g_e(1-2w^2)-2g_{\mathcal{L}}(u^2-v^2) . \end{aligned} \tag{25}$$

We see, therefore, that the effect of spin-orbit coupling to the splitoff state $|\zeta\rangle$, which yields a nonzero value for w, is to remove the axial symmetry obtained in Eq. (18).

In a study of paramagnetic resonance in transition-metal cyanides, Bleaney and O'Brien[22] in 1956 obtained expressions equivalent to Eq. (25) for the g tensor of a Kramers doublet formed as an arbitrary linear combination of t_2 orbitals appropriate to a crystal field without symmetry. We have chosen the notation θ and α for the angle variables in Eq. (23) to coincide with that used by these authors when u, v, and w are substituted into Eq. (21). As noted earlier, because Bleaney and O'Brien chose an effective-spin representation such that their states $|\pm m\rangle$ are related to $|H\rangle$ and $|H^*\rangle$ of Eq. (21) as $|+m\rangle=|H^*\rangle$, $|-m\rangle=|H\rangle$, their g values g_x, g_y, and g_z are related to those given by Eq. (25) by $g_x=g_{xx}$, $g_y=-g_{yy}$, and $g_z=-g_{zz}$. We note the inconvenience of this representation in the nearly axial case (the case of interest for the Pt^- defect) when $g_{xx}\cong g_{yy}$, since g_x and g_y then have opposite signs.

D. ^{195}Pt hyperfine interaction

Hyperfine interaction of an electron with the nuclear spin $\mathbf{I}$ of the Pt isotope ^{195}Pt has the general form[23]

$$H_H=2g_N^{\mathrm{Pt}}\mu_B\mu_N\mathbf{I}\cdot\left[\frac{\boldsymbol{\ell}}{r^3}-\frac{\mathbf{S}}{r^3}+3\frac{\mathbf{r}(\mathbf{S}\cdot\mathbf{r})}{r^5}+\tfrac{8}{3}\pi\mathbf{S}\delta(\mathbf{r})\right] , \tag{26}$$

where g_N^{Pt} is the nuclear g factor of ^{195}Pt, and μ_N is the nuclear magneton. With respect to the t_2 orbitals of Eq. (1), in the same approximation as in Eqs. (5) and (7), the first term of Eq. (26) may be represented as

$$H_H^{\mathrm{orb}}=Pg_{\mathcal{L}}(\mathcal{L}\cdot\mathbf{I}) , \tag{27}$$

where $P=2g_N^{\mathrm{Pt}}\mu_B\mu_N\langle r^{-3}\rangle_{\mathrm{Pt}}$, $g_{\mathcal{L}}$ is given by Eq. (7), and $\langle r^{-3}\rangle_{\mathrm{Pt}}$ is the one-electron average of r^{-3} with respect to the Pt $5d$ orbital ϕ_i^{Pt}. A value $P=425\times10^{-4}$ cm^{-1} is obtained for $\langle r^{-3}\rangle_{\mathrm{Pt}}=11.09$ a.u. as given for a free-ion $5d$ orbital of Pt(I) (configuration $5d^96s$) in the tables of Koh and Miller.[24]

The last term in Eq. (26) would contribute nothing for a simple d orbital, but we include an isotropic coupling (in terms of true spin $\mathbf{S}$) of the form

$$H_H^{\mathrm{con}}=A_c(\mathbf{S}\cdot\mathbf{I}) \tag{28}$$

to take into account a nonzero contact hyperfine interaction resulting from this term via the many-electron spin polarization of the Pt core electrons.[25]

The third part of the hyperfine coupling is the dipole-dipole interaction given by the second and third terms in Eq. (26), which can be represented with respect to the t_2 states by

$$\begin{aligned} H_H^{dd}=(PN^2/7)\{2[\mathcal{C}_\theta(3S_{z'}I_{z'}-\mathbf{S}\cdot\mathbf{I})+\mathcal{C}_\epsilon\sqrt{3}(S_{x'}I_{x'}-S_{y'}I_{y'})] \\ -3[\mathcal{T}_\xi(S_{y'}I_{z'}+S_{z'}I_{y'})+\mathcal{T}_\eta(S_{z'}I_{x'}+S_{x'}I_{z'})+\mathcal{T}_\zeta(S_{x'}I_{y'}+S_{y'}I_{x'})]\} , \end{aligned} \tag{29}$$

where $\mathcal{E}_\theta$, $\mathcal{E}_\epsilon$, $\mathcal{T}_\xi$, $\mathcal{T}_\eta$, and $\mathcal{T}_\zeta$ are orbital operators defined[26] in terms of the components of $\mathcal{L}$ by

$$\begin{aligned}\mathcal{E}_\theta&=(\tfrac{1}{2})(3\mathcal{L}_{z'}^2-\mathcal{L}^2)\ ,\\ \mathcal{E}_\epsilon&=(\tfrac{1}{2})\sqrt{3}(\mathcal{L}_{x'}^2-\mathcal{L}_{y'}^2)\ ,\\ \mathcal{T}_\xi&=(\mathcal{L}_{x'}\mathcal{L}_{y'}+\mathcal{L}_{y'}\mathcal{L}_{x'})\ ,\end{aligned}\tag{30}$$

etc.

Within each of the Kramers doublets (H,H^*) and (L,L^*) we represent the hyperfine interaction in the principal-axis system of the defect in terms of the effective-spin operator $\mathcal{S}$ in a form analogous to Eq. (24),

$$\mathcal{H}_H=A_{xx}\mathcal{S}_xI_x+A_{yy}\mathcal{S}_yI_y+A_{zz}\mathcal{S}_zI_z\ ,\tag{31}$$

where each of A_{xx}, A_{yy}, and A_{zz} combines the contact, orbital, and dipole-dipole interactions. For the first we obtain from Eqs. (20) and (28)

$$\begin{aligned}A_{xx}^{\rm con}&=A_c(2uv-w^2)\ ,\\ A_{yy}^{\rm con}&=A_c(2uv+w^2)\ ,\\ A_{zz}^{\rm con}&=A_c(1-2w^2)\ .\end{aligned}\tag{32}$$

The orbital interaction (27) contributes

$$\begin{aligned}A_{xx}^{\rm orb}&=-2\sqrt{2}Pg_{\mathcal{L}}w(u-v)\ ,\\ A_{yy}^{\rm orb}&=+2\sqrt{2}Pg_{\mathcal{L}}w(u+v)\ ,\\ A_{zz}^{\rm orb}&=-2Pg_{\mathcal{L}}(u^2-v^2)\ ,\end{aligned}\tag{33}$$

just as in the orbital part of the g factors in Eq. (25). Finally, the dipole-dipole contributions are found, from direct evaluation of matrix elements of $H_H^{\rm dd}$ from Eq. (29), to be

$$\begin{aligned}A_{xx}^{dd}&=(PN^2/7)[3(1-w^2)-3(u^2-v^2)\\ &\qquad -2(uv+w^2)-3\sqrt{2}w(u+v)]\ ,\\ A_{yy}^{dd}&=(PN^2/7)[-3(1-w^2)+3(u^2-v^2)\\ &\qquad -2(uv-w^2)+3\sqrt{2}w(u-v)]\ ,\\ A_{zz}^{dd}&=(PN^2/7)[2(1+w^2)+6\sqrt{2}wu]\ .\end{aligned}\tag{34}$$

Similar results for the hyperfine interaction were given previously by Bleaney and O'Brien.[22] Note that whereas the contact interaction $A_c(\mathbf{S}\cdot\mathbf{I})$ is isotropic in terms of true spin $\mathbf{S}$, it becomes anisotropic in terms of effective spin $\mathcal{S}$ accordingly to Eq. (32). By contrast, the dipole-dipole interaction is purely anisotropic in terms of true spin, each term in Eq. (29) making a zero contribution to the trace of the hyperfine tensor, while for effective spin according to Eq. (34) this trace is no longer zero.

E. ^{29}Si hyperfine interaction

Analysis of the superhyperfine interaction with the 4.7% abundant ^{29}Si nuclei on the silicon neighbors of the Pt makes it possible to determine which of the orbitals $|\alpha\rangle$ and $|\beta\rangle$ predominates in the wave function of the Kramers doublet (H,H^*) in Eq. (21) and therefore establishes the sign of θ in Eq. (15) and (16), as we will show.

We consider only the silicon nearest neighbors $k=a,b,c,d$ and take the wave functions $|\alpha\rangle$ and $|\beta\rangle$ to be as given in Eq. (2), with ϕ_k a $3s$-$3p$ hybrid bond orbital on the kth neighbor. Because $|\alpha\rangle$ is even under reflection in the $(1\bar{1}0)'$ plane (the xz plane), in which the neighbors a and d lie, ϕ_a and ϕ_d must be even under this reflection and therefore represent bonds lying in this plane. Similarly, $|\beta\rangle$ is even under reflection in the yz plane, and ϕ_b and ϕ_c represent bonds lying in this plane. Each such bond may be tilted, within the reflection plane in which it lies, with respect to the $\langle 111\rangle$ crystal direction from the Pt to the silicon neighbor. The superhyperfine interaction $H_{\rm SH}$ with respect to the orbital ϕ_k,

$$\langle\phi_k|H_{\rm SH}|\phi_k\rangle=\mathbf{S}\cdot T_k^0\cdot\mathbf{I}_k\ ,\tag{35}$$

defines a tensor T_k^0 assumed to have axial form,

$$T_k^0=\begin{bmatrix}a-b & 0 & 0\\ 0 & a-b & 0\\ 0 & 0 & a+2b\end{bmatrix}\ ,\tag{36}$$

with respect to the direction in which the bond orbital points. The reflection symmetry of ϕ_k in any case requires that the y direction be a principal axis of T_a^0 and T_d^0, however the bond is tilted, and that x be a principal axis of T_b^0 and T_c^0. The parameter a in Eq. (36) is assumed to arise via the contact interaction, as in the last term of Eq. (26), from the $3s$ part of the wave function, core polarization being neglected, and b via the dipole-dipole interaction from the $3p$ part. We then have

$$\begin{aligned}a&=(16\pi/3)g_N^{\rm Si}\mu_B\mu_N|\phi_{3s}(0)|^2p_{3s}\ ,\\ b&=(\tfrac{4}{5})g_N^{\rm Si}\mu_B\mu_N\langle r^{-3}\rangle_{\rm Si}p_{3p}\ ,\end{aligned}\tag{37}$$

where p_{3s} and p_{3p} denote the fraction of ϕ_k represented by its $3s$ and $3p$ parts, $|\phi_{3s}(0)|^2$ is the density at the nucleus of a Si $3s$ orbital, and $\langle r^{-3}\rangle_{\rm Si}$ is the average of r^{-3} with respect to a $3p$ orbital. Values for these quantities for the neutral Si atom were obtained by Watkins and Corbett,[27]

$$\begin{aligned}|\phi_{3s}(0)|^2&=31.5\times10^{24}\ {\rm cm}^{-3}\ ,\\ \langle r^{-3}\rangle_{\rm Si}&=16.1\times10^{24}\ {\rm cm}^{-3}\ ,\end{aligned}\tag{38}$$

corresponding to $a=-1380\times10^{-4}$ cm^{-1}, $b=-33.7\times10^{-4}$ cm^{-1} if p_{3s} and p_{3p} each were equal to unity in Eq. (37).

Since the orbitals $|\alpha\rangle$ and $|\beta\rangle$ involve, respectively, Si orbitals on the pairs (a,d) and (b,c), $H_{\rm SH}$ has only diagonal terms with respect to these states, found from Eqs. (1), (2), and (35) to be

$$\begin{aligned}\langle\alpha|H_{\rm SH}|\alpha\rangle&=(M^2/2)(\mathbf{S}\cdot T_a^0\cdot\mathbf{I}_a+\mathbf{S}\cdot T_d^0\cdot\mathbf{I}_d)\ ,\\ \langle\beta|H_{\rm SH}|\beta\rangle&=(M^2/2)(\mathbf{S}\cdot T_b^0\cdot\mathbf{I}_b+\mathbf{S}\cdot T_c^0\cdot\mathbf{I}_c)\ .\end{aligned}\tag{39}$$

Accordingly, we find from Eq. (21) that with respect to the doublet (H,H^*), ignoring the small admixture from the singlet $|\zeta\rangle$, the superhyperfine interaction may be represented in terms of the effective spin $\mathcal{S}$ by

$$\mathcal{H}_{\rm SH}=\sum_k \mathcal{S}\cdot T_k\cdot \mathbf{I}_k \ , \tag{40}$$

with $k=a,b,c,d$ and

$$\begin{aligned} T_a&=(M^2/2)p_\alpha^H T_a^0 \ , \\ T_b&=(M^2/2)p_\beta^H T_b^0 \ , \\ T_c&=(M^2/2)p_\beta^H T_c^0 \ , \\ T_d&=(M^2/2)p_\alpha^H T_d^0 \ , \end{aligned} \tag{41}$$

where

$$\begin{aligned} p_\alpha^H&=(u+v)^2/2\cong(\cos\theta+\sin\theta)^2/2 \ , \\ p_\beta^H&=(u-v)^2/2\cong(\cos\theta-\sin\theta)^2/2 \ . \end{aligned} \tag{42}$$

According to Eq. (2), $(M^2/2)$ is the fraction of the orbital $|\alpha\rangle$ or $|\beta\rangle$ localized on each member of the pair of Si neighbors (a,d) or (b,c), respectively, while p_α^H and p_β^H are the fractions representing the apportionment of the doublet states $|H\rangle$ and $|H^*\rangle$ between their α and β parts. It is clear from Eq. (42) that for $p_\alpha^H>p_\beta^H$ ($p_\alpha^H<p_\beta^H$) the sign of θ must be positive (negative) and, from Eq. (16), that the sign of θ is the opposite of that of $V_T Q_\xi$ (for $\lambda<0$) in the JT-distorted configuration. We note that for $\theta>0$ ($V_T Q_\xi<0$), the sense of the trigonal splitting given by Eq. (3) places $|\alpha\rangle$ at a higher energy than $|\beta\rangle$ when spin-orbit coupling is ignored. Clearly, this ordering in the trigonally distorted configuration correctly corresponds to having $p_\alpha^H>p_\beta^H$ in the upper Kramers doublet (H,H^*).

In the approximation represented by Eq. (41), the principal axes and relative anisotropies of the superhyperfine tensors T_k appropriate to the effective spin $\mathcal{S}$ are the same as those of T_k^0 appropriate to the true spin **S** for the $3s$-$3p$ hybrid on the kth neighbor. This result contrasts with the behavior of the central Pt contact and dipole-dipole interactions.

Although the symmetry axis of the tensors T_k^0 and T_k may be tipped away from a $\langle 111\rangle$ crystal axis if the $3s$-$3p$ bond is tilted, T_k^0 and T_k must retain as a plane of reflection symmetry that $\{110\}$ plane in which the Pt and its kth Si neighbor lie. Bond tilting is possible only within this plane, and its normal remains a principal axis of the hyperfine tensor. Hyperfine lines due to the neighbors a and d, which are associated with the orbital $|\alpha\rangle$ according to Eq. (39), therefore have $[1\bar{1}0]'$ (y) as a principal axis for T_a and T_d, while neighbors b and c associated with $|\beta\rangle$ have $[110]'$ (x) as a principal axis for T_b and T_c. Unambiguous identification of particular hyperfine lines with the pairs (a,d) and (b,c) is therefore possible through a study of their angular dependence.

F. Defect realignment under stress

There are six energetically equivalent orientations for a JT-distorted defect of C_{2v} symmetry in the unstrained Si lattice. These six correspond to the three $\langle 100\rangle$ crystal axes for the axis of tetragonal distortion of the defect and, for each of these, to the two possibilities for the sense of the trigonal distortion. In describing the response of these different orientations to an applied stress, we adopt the convention used in paper I (Ref. 6) of choosing the defect cubic axes (x',y',z') such that the tetragonal distortion is along z', and taking the two silicons with which hyperfine interaction is resolved to be the neighbors a and d of Fig. 3 lying in the $(1\bar{1}0)'$ plane (the xz plane of the defect principal-axis system). With the unpaired electron in the upper doublet (H,H^*) as assumed for the configuration of Fig. 2(b), this convention constrains θ to have a positive value, since it involves taking $p_\alpha^H>p_\beta^H$ in Eq. (42).

We describe the effects of macroscopic crystal strain on the orbitals $|\xi\rangle$, $|\eta\rangle$, and $|\zeta\rangle$ of Eq. (1) by

$$H_S=V_2(\epsilon_\theta \mathcal{E}_\theta+\epsilon_\epsilon \mathcal{E}_\epsilon)+V_3(\epsilon_{y'z'}\mathcal{T}_\xi+\epsilon_{z'x'}\mathcal{T}_\eta+\epsilon_{x'y'}\mathcal{T}_\zeta) \ , \tag{43}$$

where V_2 and V_3 are strain-coupling coefficients,[26] ϵ_{mn} is a component of the strain tensor, ϵ_θ and ϵ_ϵ are defined as

$$\begin{aligned} \epsilon_\theta&=\epsilon_{z'z'}-(\tfrac{1}{2})(\epsilon_{x'x'}+\epsilon_{y'y'}) \ , \\ \epsilon_\epsilon&=(\sqrt{3}/2)(\epsilon_{x'x'}-\epsilon_{y'y'}) \ , \end{aligned} \tag{44}$$

and $\mathcal{E}_\theta$, $\mathcal{E}_\epsilon$, $\mathcal{T}_\xi$, $\mathcal{T}_\eta$, and $\mathcal{T}_\zeta$ are the operators defined in Eq. (30).

The relative shift in energy ΔE_i of the ith defect orientation with strain (a common shift due to dilatation being omitted) may be expressed as

$$\Delta E_i=\sum_{m,n} B_{mn}\epsilon_{mn}^i \ , \tag{45}$$

where B_{mn} is a component of the piezospectroscopic tensor[28] of the defect defined in the defect cubic axis system, and ϵ_{mn}^i is a component of the strain tensor for the ith orientation with respect to these axes. In order to express B_{mn} in terms of V_2 and V_3, we evaluate the response of the Kramers doublets (H,H^*) and (L,L^*) to an arbitrary strain, using H_S from Eq. (43) and wave functions from Eqs. (15) and (A1) [or, equivalently, Eqs. (21), (23), and (A3)], and making the approximation $\alpha=0$,

$$\langle H|H_S|H\rangle=\tfrac{1}{2}V_2\epsilon_\theta-V_3\epsilon_{x'y'}\sin 2\theta \ , \tag{46}$$

$$\langle L|H_S|L\rangle=\tfrac{1}{2}V_2\epsilon_\theta+V_3\epsilon_{x'y'}\sin 2\theta \ , \tag{47}$$

terms involving ϵ_ϵ, $\epsilon_{y'z'}$, and $\epsilon_{z'x'}$ making no contribution to either expression. Since for Pt^- the lower doublet (L,L^*) is doubly occupied while (H,H^*) contains a single electron, we add $2\langle L|H_S|L\rangle$ to $\langle H|H_S|H\rangle$ and compare the resulting expression with Eq. (45), obtaining

$$B_{z'z'}=-2B_{x'x'}=-2B_{y'y'}=+\tfrac{3}{2}V_2 \ , \tag{48}$$

$$\begin{aligned} B_{x'y'}&=B_{y'x'}=\tfrac{1}{2}V_3\sin 2\theta \ , \\ B_{y'z'}&=B_{z'y'}=B_{z'x'}=B_{x'z'}=0 \ . \end{aligned} \tag{49}$$

Consider a compressional unaxial stress P along a $\langle 110\rangle$ direction as in the experiments described in paper I. For the two defect orientations with their tetragonal axes perpendicular to this stress direction we have

$$\epsilon^i_\theta=\tfrac{1}{2}(s_{11}-s_{12})P\ ,$$
$$\epsilon^i_{x'y'}=\pm s_{44}P/4\ , \tag{50}$$
$$\epsilon^i_\epsilon=\epsilon^i_{y'z'}=\epsilon^i_{z'x'}=0\ ,$$

where s_{11}, s_{12}, and s_{44} are the elastic compliance constants of silicon. The plus sign in $\epsilon^i_{x'y'}$ goes with that orientation A (see Ref. 6, Fig. 2) for which the uniaxial stress is in the direction $[1\bar{1}0]'$ (y), and the minus sign with orientation B for which the stress is along $[110]'$ (x). For orientation A, the total-energy shift under this stress is therefore

$$\Delta E_A=+\tfrac{3}{4}PV_2(s_{11}-s_{12})+\tfrac{1}{4}PV_3s_{44}\sin2\theta\ , \tag{51a}$$

from Eq. (45), while for the orientation B,

$$\Delta E_B=+\tfrac{3}{4}PV_2(s_{11}-s_{12})-\tfrac{1}{4}PV_3s_{44}\sin2\theta\ . \tag{51b}$$

The energies of the remaining four orientations $(i=C,D,E,F)$, which have their tetragonal axis at 45° to the stress direction and for which $\epsilon^i_{x'y'}=0$, are shifted equally by the stress,

$$\Delta E_{C-F}=-\tfrac{3}{8}PV_2(s_{11}-s_{12})\ . \tag{52}$$

G. Relation of JT energies to strain-coupling coefficients

To relate the strain-coupling coefficients V_2 and V_3 to the JT coupling, we adopt the usual cluster model,[29] or quasimolecular model,[30] in which the splitting of the electronic degeneracy of the defect is assumed the result only of the relative displacements of the Pt and its nearest neighbors. The usual treatment, assuming nearest neighbors of Pt displaced by strain just as in bulk silicon (e.g., that the local elastic constants are unchanged by the presence of the defect), leads to relations[31] between V_2,V_3 and the JT coupling coefficients[26] V_E,V_T for the t_2 orbitals,

$$V_E=V_2\sqrt{6}/a\ ,$$
$$V_T=V_3\sqrt{2}/a\ , \tag{53}$$

where $a=5.43$ A is the lattice constant of silicon.

Taking account of the triple occupancy of the t_2 orbitals in Fig. 2(b), we have for the energy of the ground state of Pt^- as a function of the tetragonal distortion mode Q_θ, relative to that of the undistorted tetrahedral configuration,

$$E=\tfrac{3}{2}V_EQ_\theta+(k_E/2)Q_\theta^2\ , \tag{54}$$

where k_E is the relevant force constant. The JT stabilization energy for the tetragonal mode, as given by the minimum of Eq. (54), is then

$$(E_{JT})_{\rm tet}=(9V_E^2/8k_E)=(27V_2^2/4a^2k_E)\ , \tag{55}$$

which occurs at the distortion $Q_\theta=-3V_E/2k_E$. In this tetragonally distorted configuration, the one-electron energy difference Δ_ξ between the doublet $|\xi\rangle$, $|\eta\rangle$ and the excited singlet $|\zeta\rangle$ is

$$\Delta_\xi=-\tfrac{3}{2}V_EQ_\theta=\tfrac{9}{4}(V_E^2/k_E)=2(E_{JT})_{\rm tet}\ . \tag{56}$$

The additional stabilization energy caused by JT coupling to the trigonal mode as given by Eq. (3) would be

$$(E_{JT})^0_{\rm trig}=V_T^2/2k_T=V_3^2/a^2k_T \tag{57}$$

if spin-orbital coupling could be neglected. Spin-orbit coupling acts to reduce the instability of the tetragonally distorted configuration with respect to Q_ξ and eliminates it completely if $|\lambda|$ is large enough. The energy of the configuration with two electrons in (L,L^*) and one in (H,H^*) as a function of Q_ξ is found from Eqs. (14) and (17) to be

$$E=-(3\lambda/2\sqrt{2})\tan\alpha-\tfrac{1}{2}[\lambda^2(1+2^{-1/2}\tan\alpha)^2+4V_T^2Q_\xi^2\cos^2\alpha]^{1/2}+\tfrac{1}{2}k_TQ_\xi^2\ . \tag{58}$$

This has a maximum at $Q_\xi=0$, so that this configuration is unstable, if the inequality

$$(V_T\cos\alpha)^2/k_T>(|\lambda|/2)(1+2^{-1/2}\tan\alpha) \tag{59}$$

is satisfied. Minima then occur for distortions $\pm|Q_\xi|$ corresponding to values for θ in Eq. (16) given by

$$\cos2\theta=-(\lambda/2)(1+2^{-1/2}\tan\alpha)/(V_T^2\cos^2\alpha/k_T)\ . \tag{60}$$

The energy at these minima with respect to the tetragonally distorted configuration is then $-(E_{JT})_{\rm trig}$, with

$$(E_{JT})_{\rm trig}=\cos^2\alpha(1-|\cos2\theta|)^2(E_{JT})^0_{\rm trig} \tag{61}$$

the spin-orbit-corrected trigonal JT energy.

III. VACANCY MODEL COMPARED TO EXPERIMENT

A. EPR parameters

Table I lists the experimental g factor and central hyperfine parameters for Pt^- in Si, taken from Table I of paper I (Ref. 6). We note that the g factor is nearly of axial symmetry with respect to the z axis, so that it is convenient to form from Eq. (25)

$$\tfrac{1}{2}(g_{xx}+g_{yy})=g_e2uv+g_\perp2\sqrt{2}wv\ , \tag{62}$$

which has the experimental value 1.4065. Assuming the second term in Eq. (62) to be negative and of order 0.01

TABLE I. Experimental g factor and Pt hyperfine coupling parameters, appropriate to the spin Hamiltonians of Eqs. (24) and (31), for the Pt^- defect in silicon. Tabulated values are taken from Table I of Ref. 6 and are referred to the principal-axis system of the defect, in which the principal hyperfine coupling with neighboring ^{29}Si occurs at the two nearest-neighbor sites lying in the xz plane.

Component ij	xx	yy	zz
g_{ij}	1.3865	1.4265	2.0789
A_{ij} (10^{-4} cm^{-1})	148	186	127

or smaller, we have then approximately

$$2uv \cong \sin 2\theta \cong 0.71 \ , \tag{63a}$$

and therefore from Eq. (23)

$$u^2 - v^2 \simeq \cos 2\theta \cong 0.704$$

$$u \cong \cos\theta \cong 0.923 \ , \tag{63b}$$

$$v = \sin\theta \cong 0.385 \ .$$

We use these approximate values in the following analysis.

First we note that these values for $\cos\theta$ and $\sin\theta$ are consistent with the experimental observation[6] that the resolved hyperfine interaction is with ^{29}Si on only two of the four nearest-neighbor sites. Substituting into Eq. (42), we have $p_\alpha^H = 0.86$, $p_\beta^H = 0.14$. The orbital $|\alpha\rangle$ therefore strongly predominates over $|\beta\rangle$ in the Kramers doublet (H, H^*), and the ^{29}Si hyperfine coupling at sites b and c is predicted to have a value only about one-sixth that at sites a and d. Partially resolved shoulders observed[2,3,6] (see Fig. 3 of paper I) on the resonance lines are consistent with such an estimate for the coupling at this second pair of sites, but their intensities suggest that additional sites with comparable coupling may also be contributing. This broadening has been suggested by Henning and Egelmeers[2] to be the result of hyperfine coupling to a second Pt atom, but this suggestion is not supported by the studies of Milligan, Anderson, and Watkins[3,6] on samples isotopically enriched in ^{195}Pt or ^{198}Pt.

Since interpretation of the EPR parameters depends strongly on what is assumed for the extent of the spin-orbit mixing with the splitoff state $|\zeta\rangle$, we try different choices for the coefficient w of $|\bar{\xi}\rangle$ in the state $|H\rangle$ of Eq. (21). [We expect to have $w > 0$ from Eqs. (13) and (23).] Equation (25) for g_{zz} and the experimental value 2.079 then yield the values for $g_\perp$ given in Table II, which from Eq. (7) should equal $-N^2$. The localization of the wave function on the central Pt atom is therefore in the range 5–12 % for w in the range $0 \le w \le 0.15$.

We may obtain a separate estimate of N^2 from the Pt hyperfine interaction. From Eqs. (32), (33), and (34), setting $g_\perp = -N^2$ in the orbital terms, we can write

$$A_{zz} = A_c(1-2w^2) + PN^2[2(u^2-v^2) + (\tfrac{2}{7})(1+w^2) + (6\sqrt{2}/7)wu] \ , \tag{64}$$

$$\tfrac{1}{2}(A_{xx} + A_{yy}) = A_c 2uv - PN^2(\tfrac{2}{7}uv + \tfrac{17}{7}\sqrt{2}wv) \ , \tag{65}$$

and thus obtain two equations that can be solved simultaneously for A_c and PN^2. We assume the experimental values of A_{xx}, A_{yy}, and A_{zz} to be negative (these signs not having been determined experimentally) in the expectation that A_c should be negative while PN^2 is positive. Accordingly, from $A_{zz} = -127 \times 10^{-4}$ cm^{-1}, $\frac{1}{2}(A_{xx} + A_{yy}) = -167 \times 10^{-4}$ cm^{-1} we obtain the values for A_c and PN^2 given in Table II. A_c and PN^2 are therefore in the neighborhood of -220×10^{-4} and $+50 \times 10^{-4}$ cm^{-1}, respectively. Taking $P = 425 \times 10^{-4}$ cm^{-1} for a Pt $5d$ orbital,[24] we have then an independent determination of N^2 as shown in Table II. This is of the same order of magni-

TABLE II. Values obtained for various parameters in Eqs. (25) and (64)–(67) by fitting these theoretical expressions to the experimental values for the g factors and Pt hyperfine parameters (Table I), using different assumed values of the cofficient w in the wave function of Eq. (21). See Sec. III A for procedures used and for discussion.

w	$g_\perp$	A_c (10^{-4} cm^{-1})	PN^2 (10^{-4} cm^{-1})	N^2	$\frac{6}{7}PN^2(1-\cos 2\theta)$ (10^{-4} cm^{-1})	$-2w^2(A_c + \frac{5}{7}PN^2)$ (10^{-4} cm^{-1})	$\frac{22}{7}\sqrt{2}PN^2 w\cos\theta$ (10^{-4} cm^{-1})	$A_{xx} - A_{yy}$ (10^{-4} cm^{-1})	$-2g_e w^2$	$-g_\perp 4\sqrt{2}w\cos\theta$	$g_{xx} - g_{yy}$
0.0	−0.055	−227	59	0.14	14.9	0	0	15	0	0	0
0.05	−0.062	−222	54	0.13	13.7	0.9	11.1	26	−0.010	0.016	0.006
0.10	−0.083	−219	49	0.12	12.3	3.7	19.9	36	−0.040	0.043	0.003
0.15	−0.12	−216	45	0.11	11.4	8.3	27.7	47	−0.090	0.093	0.003

tude as that obtained previously from $-g_{\mathcal{L}}$.

The anisotropy in the hyperfine interaction may be given from Eqs. (32), (33), and (34) as

$$A_{xx}-A_{yy}=\tfrac{6}{7}PN^2[1-(u^2-v^2)]-2w^2(A_c+\tfrac{5}{7}PN^2)+\tfrac{22}{7}\sqrt{2}PN^2wu\ . \quad (66)$$

Each of these three terms in this equation, listed separately in Table II together with their sum, is unambiguously positive for $w>0$ so long as A_c is negative and greater in magnitude than $\frac{5}{7}PN^2$. The experimental difference $A_{xx}-A_{yy}=38\times10^{-4}$ cm^{-1} is therefore of the predicted sign, and it agrees in magnitude with the model if w has a value ~0.1.

The g-factor departure from axial symmetry,

$$g_{xx}-g_{yy}=-2g_e w^2-g_{\mathcal{L}}4\sqrt{2}wu \quad (67)$$

from Eq. (25), should be positive if the orbital term dominates, but may be reversed in sign by the w^2 correction to the spin term. The calculated values of these terms in Table II nearly cancel, but the sum remains positive when the values of $g_{\mathcal{L}}$ previously determined are used, whereas the experimental value $g_{xx}-g_{yy}=-0.04$ is negative. We note that the anisotropy $g_{xx}-g_{yy}$ arises solely from the spin-orbit mixing with the state $|\zeta\rangle$, in contrast to the hyperfine anisotropy $A_{xx}-A_{yy}$, which has a large zero-order contribution from the dipole-dipole coupling. However, $A_{xx}-A_{yy}$ also has a large contribution from the spin-orbit mixing, so that the failure of this prediction for $g_{xx}-g_{yy}$ means that we cannot reliably use the hyperfine anisotropy to determine w in the manner suggested above. We note that coupling with other states outside the t_2 gap manifold (in particular, the Pt orbital doublet $E\theta$ and $E\epsilon$ states, which together with the t_2 states make up the Pt d levels) can also contribute to the anisotropy in both g and A. Such additional coupling must play a significant role for Pt$^-$ but is not included in the present model.[32]

A localization $N^2\simeq10\%$ would lead us to expect from Eq. (5) a spin-orbit parameter $\lambda\simeq-340$ cm^{-1} if the Pt wave function is approximated by a $5d$ atomic orbital. This in turn is consistent with $w\sim0.1$ from Eqs. (13) and (23) if we should have $\Delta_\zeta\sim0.30$ eV for the excitation energy of the state $|\zeta\rangle$. (We attempt to estimate Δ_ζ in Sec. III B.) Uncertain as these estimates may be, they are qualitatively consistent with the assumptions of the vacancy model. The contact term in the Pt hyperfine interaction appears anomalous in this regard, however, because the result $A_c\simeq-220\times10^{-4}$ cm^{-1} yields for the ratio $|A_c|/P$ a value ~0.5 similar to that inferred by Simanek *et al.*[33] for Pt^{3+} in $BaTiO_3$, a host in which the wave function should be much more localized on the impurity. A calculation of core polarization for the $5d$ group of transition metals by Freeman, Mallow, and Bagus[34] gave for this ratio a value near unity for the Pt^{2+} ion, so that a value ~0.1 would have been expected for Pt$^-$ in silicon if the s electron spin density at the Pt nucleus scaled simply with N^2. Such a scaling evidently cannot be assumed, presumably because spin polarization of the deep molecular bonding d orbitals in the valence band can contribute significantly to the spin density localized on the Pt. Such an effect has been noted in theoretical calculations,[35,36] where the spin density at the impurity nucleus is affected strongly by exchange polarization of the filled valence-band states and can be large even though the partially filled orbitals in the gap are relatively delocalized.

The fraction of the wave function localized at nearest-neighbor sites may be established from the measured ^{29}Si hyperfine coupling as given in Table I of paper I. Referring this coupling to the principal axis system of the Si hyperfine tensor, we have 36.9×10^{-4} and 27.0×10^{-4} cm^{-1} for the principal values in the xz plane, with the bond directions at the sites a and d tipped by $\pm10.4°$ with respect to the x axis.[6] The hyperfine tensor is approximately axial with respect to the bond direction, as assumed in Eq. (36), and we find, corresponding to Eqs. (38) and (41), that we have $(M^2/2)p_{3s}p_\alpha^H\cong0.021$, $(M^2/2)p_{3p}p_\alpha^H\simeq0.108$. Thus 2.1% and 10.8% of the wave function of the state (H,H^*) appears as localized in the $3s$ and $3p$ Si orbitals, respectively, at each of the two nearest-neighbor sites that give a resolved hyperfine structure. With $p_\alpha^H=0.86$, $p_\beta^H=0.14$ from Eqs. (42) and (63), we should have 0.3% and 1.8% in the corresponding orbitals at the other two nearest-neighbor sites, for a total of 30% at these four sites. With $\sim10\%$ localization at the Pt, the model thus accounts for $\sim40\%$ of the electron density, the remainder presumably being distributed over more distant neighbors. A roughly similar distribution was obtained in the theoretical cluster-model calculations for Pt$^-$ by Alves and Leite.[15]

B. Strain-coupling coefficients and JT energies

Table III shows the strain-coupling coefficients for Pt$^-$ in Si as measured in paper I (Ref. 6), together with those of the three charge states V^-, V^0, and V^+ of the isolated vacancy.[13] We note that $B_{z'z'}$ for Pt$^-$ has the opposite sign from that for V^-. Comparing with Eq. (48), we ob-

TABLE III. Experimental strain-coupling coefficients for Pt$^-$ and for the charge states of the isolated vacancy in silicon.

	$B_{z'z'}=-2B_{x'x'}=-2B_{y'y'}$ (eV)	$B_{x'y'}=B_{y'x'}$ (eV)	Ref.
Pt$^-$	+4.12	+2.68	Paper I
V^-	−9.9	−7.2	13
V^0	−13.3		13
V^+	−6.5		13

tain $V_2=2.75$ eV for the one-electron strain-coupling coefficient for Pt^- corresponding to the electronic configuration shown in Fig. 2(b). By contrast, the configuration for V^- shown in Fig. 2(a) leads to a relationship identical with Eq. (48) except in having the sign reversed, so that we obtain $V_2=6.6$ eV for V^-. The one-electron strain-coupling coefficient V_2 therefore has the same sign for V^- and Pt^- if Figs. 2(a) and 2(b), respectively, describe these centers. The reversal of the sense of the tetragonal JT distortion for Pt^- as compared to V^-, as proposed by the vacancy model for Pt^-, is therefore supported by this result. The magnitude of V_2 for Pt^- is, however, only 42% of that for V^-, indicating a significant effect of the presence of the central platinum ion on the properties of the vacancy.

The signs of $B_{x'y'}=B_{y'x'}$ for Pt^- and V^- in Table III are also opposite. From Eq. (49) for Pt^-, taking $\sin 2\theta=0.71$ from Eq. (63a), we obtain then $V_3=7.5$ eV for the one-electron coupling coefficient for the trigonal strain. For V^-, on the other hand, Fig. 2(a) shows that we have but a single electron occupying orbitals $|\xi\rangle$ and $|\eta\rangle$, so that the entry for $B_{x'y'}$ in Table III corresponds in the trigonally distorted configuration to a single electron in the orbital $|\alpha\rangle$, spin-orbit interaction being very weak for the vacancy. Since we have $-V_3\epsilon_{x'y'}$ for the $\epsilon_{x'y'}$ part of $\langle\alpha|H_S|\alpha\rangle$ from Eq. (43), we accordingly obtain $V_3=-2B_{x'y'}=14.4$ eV from Eq. (45) and Table III. We find, therefore, that the one-electron strain-coupling coefficient V_3 has the same sign for V^- as for Pt^-, as expected for the vacancy model. As for the coupling to tetragonal strain, we find V_3 reduced in magnitude for Pt^- as compared to V^- by $\sim 50\%$.

These values for V_2 and V_3 are collected in Table IV, together with those for V^+ and V^0 from the data of Table III for the configurations with one or two electrons in the orbital $|\xi\rangle$, respectively. Watkins[13] has previously used these parameters for the vacancy in estimating the corresponding JT energies from Eqs. (55) and (57) for V^- [and from corresponding expressions for V^+ and V^0, for which the numerical coefficients should be 3 and 12, respectively, in place of 27/4 in Eq. (55)]. Watkins used the estimate $k_E=2k_T=11.9$ eV/A^2 for the force constants. These estimates are reproduced in Table IV. Taking for Pt^- the same values of the force constants, we obtain the corresponding JT energies for Pt^- also given in Table IV. The trigonal JT energy for Pt^-, when corrected for spin-orbit coupling as in Eq. (61), would, of course, be substantially smaller than the tabulated value for $(E_{JT})^0_{trig}$.

The estimate $(E_{JT})_{tet}\cong 0.15$ eV is consistent according to Eq. (56) with the observation made in Sec. III A that a value $\Delta_\xi\cong 0.3$ eV would be compatible with a value $w\cong 0.1$ for the coefficient of $|\zeta\rangle$ or $|\bar{\zeta}\rangle$ in Eq. (21) if we have $\lambda\simeq -340$ cm^{-1}. The value $(E_{JT})^0_{trig}=0.3$ eV is much too large, however, to be consistent with Eq. (60) and the value $\cos 2\theta\cong 0.7$ if λ is of this magnitude. As Watkins[13] has noted, the values of $(E_{JT})_{tet}$ in Table IV for the vacancy charge states almost certainly overestimate this quantity by a factor ~ 2, to judge from the success of the theoretical calculations of Baraff, Kane, and Schlüter[37] in predicting energies of the single- and double-donor levels of the vacancy and in accounting for its negative-U behavior. An overestimate for the value in Table IV of $(E_{JT})^0_{trig}$ for V^-, by a factor somewhat larger than 2, also undoubtedly occurs, since otherwise the principal JT distortion of all the charge states of the vacancy should be trigonal instead of tetragonal as observed. The JT energies for Pt^- given in Table IV are therefore likely to be too large. Such overestimates for JT energies, when obtained from strain-coupling coefficients, are often encountered in studies of the JT effect and presumably represent a failure of the cluster model, as discussed by Hjortsberg, Vallin, and Ham in the case of Fe^{2+} in MgO.[38]

TABLE IV. One-electron strain-coupling coefficients and Jahn-Teller energies (without spin-orbit correction) calculated from these coefficients (with $k_E=2k_T=11.9$ eV/A^2) for Pt^- and for the isolated vacancy in silicon.

	Pt^-	V^-	V^0	V^+
V_2 (eV)	2.75	6.6	6.65	6.5
V_3 (eV)	7.5	14.4		
$(E_{JT})_{tet}$ (eV)	0.15	0.9	1.5	0.4
$(E_{JT})^0_{trig}$ (eV)	0.3	1.2		

IV. ALTERNATIVE MODELS

Alternative models to account for the paramagnetic behavior of Pt^- in Si have been proposed by Lowther[7] and by Ammerlaan and van Oosten.[8] These hold in common with the vacancy model that the properties of the defect can be approximated by a state formed as a linear combination of t_2 orbitals (effective p states) in orthorhombic (C_{2v}) symmetry. The first of these, proposed by Lowther in 1980,[7] takes the Pt d shell to be diamagnetic and associates the resonance with a hole occupying a bonding molecular orbital. As in our work, the spin-orbit interaction was interpreted as comparable in strength to the trigonal (orthorhombic) component of the crystal field, and the orbital g factor was found to be small (~ 0.06), supposedly as a result of the combined effects of hole delocalization and a dynamic JT effect. Lowther proposed his model to explain the observed g-factor anisotropy, and his work did not address the hyperfine interaction with either the Pt or its neighboring Si or attempt to show how the spontaneous distortion of the defect from tetrahedral symmetry might result from JT coupling of the hole.

The model of Ammerlaan and van Oosten[8] followed a suggestion of Woodbury and Ludwig[1] in assuming the Pt d shell to be in the $5d^9$ configuration, with the Pt covalently bonded via 6s and 6p orbitals to two neighboring Si. The remaining two Si neighbors were assumed bonded to each other by a reformed bond, so that six of the defect's electrons are taken up by these three bonds, leaving the nine remaining electrons of Pt^- in the 5d shell. The paramagnetic properties of the center were thus assumed to be those of a single 5d hole as perturbed by a crystal field of C_{2v} (dihedral or orthorhombic) symmetry. If the hole is taken to be in one of the t_2 5d orbitals, Am-

merlaan and van Oosten asserted that the experimental g factors determine uniquely the ratio of the two independent parameters of the crystal field (the tetragonal and trigonal components) to the spin-orbit parameter. They concluded in addition that the resulting model is incompatible with the vacancy model in that the hole is 73% localized in the Pt $5d$ orbital.

The signs of the Pt$^-$ g factors g_{xx}, g_{yy}, and g_{zz} were not determined in the original experiments of Woodbury and Ludwig[1] or in subsequent studies,[2-6] and Ammerlaan and van Oosten[8] concluded that the EPR data can be fitted to their $5d^9$ dihedral model only if all are taken to be negative. By contrast, in the model proposed in the present work, g_{zz} is given by the theory to be positive according to Eq. (18) or (25), while g_{xx} ad g_{yy} are either both positive or both negative depending on the sign of θ. We can change the sign of any two of the three g_{ii} by an appropriate trivial change in the basis used in defining the effective spin in Eq. (19), as discussed briefly in Sec. II C, but the sign of the product $g_{xx}g_{yy}g_{zz}$ is invariant. The sign of this product in principle may be established in an EPR experiment designed to determine whether right- or left-circularly polarized microwave radiation is preferentially absorbed.[39] Such an experiment would therefore be crucial to determine if this product has the sign assumed by Ammerlaan and van Oosten[8] in proposing their $5d^9$ dihedral model or that given by our interpretation based on the vacancy model.

It is of interest to contrast the crystal-field parameters obtained in the $5d^9$ dihedral model with those of the vacancy model. Figure 5 is taken from the paper of Ammerlaan and van Oosten[8] and shows the splitting of a $^2T_2$ state of a single hole under the combined effect of spin-orbit interaction [as in Eq. (4) with $\lambda>0$ for a single $5d$ hole] and a tetragonal distortion δ_{te} [which equals the ratio Δ_ζ/λ in Eq. (13)]. We have labeled the Kramers doublets $n=1,2,3$ of Ammerlaan and van Oosten according to the states $|\zeta\rangle$, $|A\rangle$, and $|B\rangle$ from Eqs. (8) and (9) with which they may be identified for $|\delta_{te}|\gg1$. We have also added a solid arrow to indicate the value $\delta_{te}=0.302$ at which Ammerlaan and van Oosten found the g factors of the $n=1$ level of the dihedral model to fit the Pt$^-$ data. We note that this arrow represents only a small departure from the case of perfect tetrahedral symmetry ($\delta_{te}=0$), at which the lower level is the $J=\frac{1}{2}$ spin-orbit level (the $J=\frac{3}{2}$ level being the upper level at this point). The trigonal (orthorhombic) distortion determined by Ammerlaan and van Oosten from the g-factor anisotropy $g_{xx}-g_{yy}$ was found to be even smaller, $\delta_{rh}=0.007$ (where δ_{rh} corresponds to the ratio V_TQ_ζ/λ of our parameters in the stable configuration of the trigonal JT distortion mode). By contrast, the doublets (H,H^*) and (L,L^*) of Eq. (15) and the Appendix correspond to the far right-hand side of Fig. 5 ($\delta_{te}\gg1$) when the mixing of the A and B doublets by the distortion Q_ζ is included. The discussion of Ammerlaan and van Oosten overlooks the fact that a nearly axial EPR spectrum with $g_{xx}\cong g_{yy}\neq0$ can also result in their model from this region ($\delta_{te}\gg1$) of Fig. 5 when the mixing of the doublets 1 and 3 (A and B) through an orthorhombic distortion δ_{rh} is included. The anisotropy $(g_{xx}-g_{yy})\neq0$ appears in this situation only through spin-orbit coupling to the splitoff state $|\zeta\rangle$, as shown by our analysis of Sec. II B and the Appendix, and is therefore small so long as we have $\delta_{te}\gg1$. Indeed, the ground-state doublet (L,L^*) of a one-hole model in this regime has $g_{xx}g_{yy}g_{zz}>0$ according to Eq. (A2). This opens another possibility, not considered by Ammerlaan and van Oosten, for interpreting the Pt$^-$ data on the basis of the $5d^9$ dihedral model. We have determined that this doublet (L,L^*) in fact reproduces the experimental g factors if the parameters in Eq. (A3) take values $u=0.9229$, $v=0.3793$, $w=-0.0657$ for $g_\perp=-0.0664$. These values correspond to $\tan\theta=-2.439$, $\tan\alpha=0.0712$ in Eqs. (13) and (16), from which we obtain $\delta_{te}=\Delta_\zeta/\lambda=9.382$, $\delta_{rh}=V_TQ_\zeta/\lambda=0.519$. This value for δ_{te} is indicated by the dashed arrow on the right-hand side of Fig. 5. In this model the value obtained for $g_\perp$ denotes a hole wave function only $\sim7\%$ localized in the Pt d orbitals, similar to what we found for the vacancy model in Sec. III A but in contrast to the 73% localization found by Ammerlaan and van Oosten. However, with the above values for u,v,w in Eq. (A3), we are unable to account for the anisotropy in the Pt hyperfine interaction, the value for $A_{xx}-A_{yy}$ obtained from Eq. (66) being smaller than the experimental value by at least an order of magnitude for any reasonable values for A_c and PN^2. We have found the same discrepancy for the Pt hyperfine coupling for the parameters of the model of Ammerlaan and van Oosten.

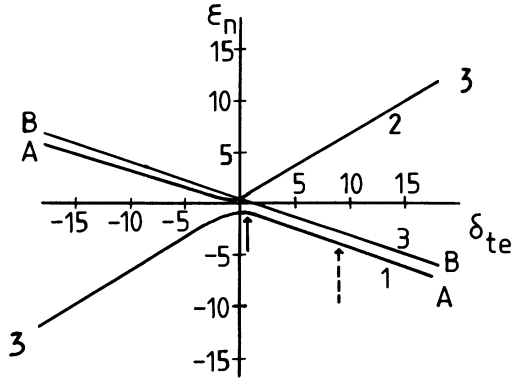

FIG. 5. Splitting of a $^2T_2$ state of a single t_2 hole under the combined effect of spin-orbit coupling and a tetragonal distortion (after Ref. 8). Ratios of the energy E and the crystal-field splitting Δ_ζ to the spin-orbit parameter λ ($\lambda>0$) are denoted by ϵ_n and δ_{te}. Kramers doublets are labeled $n=1,2,3$ as in Ref. 8 and are identified with the singlet $|\zeta\rangle$ and the spin-orbit states $|A\rangle$ and $|B\rangle$ of Eqs. (8) and (9) for $|\delta_{te}|\gg1$. Arrows indicate values for δ_{te} at which g factors of the $n=1$ level match experimental values for Pt$^-$ according to alternative interpretations based on the $5d^9$ dihedral model (see text).

This second interpretation of the g-factor anisotropy in terms of the $5d^9$ dihedral model indeed appears to correspond to Lowther's model[7] for Pt$^-$, although the required sign of the orbital g factor $g_\perp$ is the opposite of that given by Lowther. In his model, Lowther took for his parameters the values $k_z=0.06$, $\lambda_\perp k_\perp/E\cong0.015$,

$\lambda_z/\Delta=0.90$, which in our notation (where, in contrast to Lowther, we have made no distinction between orbital g factors and spin-orbit parameters associated with components parallel and perpendicular to the tetragonal axis of distortion) should correspond to taking $g_{\mathcal{L}}=0.06$, $\lambda g_{\mathcal{L}}/\Delta_\zeta \cong 0.015$, $\lambda/2V_T Q_\zeta=0.90$. With these values we obtain $u=0.903$, $v=0.407$, $w=-0.139$ for the coefficients in the Kramers doublet (L,L^*) from Eq. (A3), but according to Eq. (25) one then finds $g_{zz}<2$, in contrast to the experimental value $g_{zz}=2.079$. If, however, we change the sign of Lowther's k_z to give $g_{\mathcal{L}}=-0.06$, as might be expected for a t_2 state containing an admixture from the Pt $5d$ shell, but keep $\lambda/\Delta_\zeta \simeq 0.25$ ($\lambda>0$), we find that Lowther's parameters yield the correct signs for both $(g_{zz}-2)$ and $(g_{xx}-g_{yy})$. The numerical fit to the experimental values is poor, however, evidently because Lowther omitted all but first-order terms in $\lambda_\perp/E$ in fitting his theory to the data. With this change, his parameters would correspond to $\delta_{te}=4.0$, $\delta_{rh}=0.55$ in the $5d^9$ dihedral model, which thus approximates the alternative situation we have described ($\delta_{te}=9.382$, $\delta_{rh}=0.519$), which does reproduce the experimental g-factor anisotropy but not that of the Pt hyperfine coupling.

In order that hyperfine coupling with the neighboring Si occur principally at the sites a and d rather than at b and c, the defect's wave function must be predominantly formed from the orbital $|\alpha\rangle$ from Eq. (2), which is even under reflection in the xz plane. As we have seen in Eq. (21), spin-orbit interaction mixes $|\alpha\rangle$ with $|\beta\rangle$, which is odd under this reflection and gives hyperfine coupling at b and c. Predominant coupling at a and d therefore requires $p_\alpha^L \gg p_\beta^L$ from Eq. (A4), or equivalently $(u+v)^2 \gg (u-v)^2$ in terms of the wave-function coefficients u and v. This condition is reasonably well satisfied for $\delta_{te}=9.382$, $\delta_{rh}=0.519$ in the $5d^9$ dihedral model, for which we have $(u+v)^2/(u-v)^2=5.74$. But for the situation considered by Ammerlaan and van Oosten[8] with $\delta_{te}=0.302$, $\delta_{rh}=0.007$, we find $u=0.864$, $v=0.004$, $w=-0.503$, yielding $(u+v)^2/(u-v)^2=1.02$. Such a state could satisfy the requirement of predominant hyperfine coupling at a and d only if, through covalent bonding of Pt with the Si, $|\alpha\rangle$ had much greater amplitude at a and d than $|\beta\rangle$ has at b and c. However, $|\alpha\rangle$ and $|\beta\rangle$ must be equivalent orbitals, related to each other by an improper $\pi/2$ rotation about z, in the tetragonal configuration ($\delta_{rh}=0$), so that any difference in their bonding can result only from the orthorhombic distortion. It is unlikely that the very small energy difference $2\Delta_{rh}=4.4$ meV inferred by Ammerlaan and van Oosten corresponding to $\delta_{rh}=0.007$ could represent the energy difference of such orbitals if one had significant bonding to two Si atoms while the other did not.

Theoretical calculations for substitutional transition-metal impurities in silicon have shown that at the heavy end of the series the d levels are deep in the valence band or below it,[10–12,15] and the vacancy model for Pt is based on this assumption, with the t_2 gap manifold of states having only a small localization in the Pt $5d$ orbitals. In the $5d^9$ dihedral model of Ammerlaan and van Oosten,[8] the Pt $5d$ states, by contrast, would have to be sufficiently shallow that this shell retains a hole that is strongly localized on the Pt. Their interpretation, moreover, assumes that the form of the spontaneous dihedral distortion is due to the covalent bonding of the Pt $6s$ and $6p$ orbitals with two neighboring Si atoms rather than to the JT coupling of the t_2 hole. Indeed, for a single such hole, one would expect a spontaneous tetragonal JT distortion to have the opposite sense in Fig. 5 (i.e., to be to $\delta_{te}<0$ so that $|\zeta\rangle$ is the ground state) from that indicated by the fit to the g factors, and the additional orthorhombic distortion would not then be expected to occur. If this orthorhombic distortion is due to the covalent bonding of the $6s$ and $6p$ Pt orbitals with the two Si neighbors, as postulated in the $5d^9$ dihedral model, it is then remarkable that rapid reorientation of this distorted complex can occur at ~ 2 K, as observed in the experiments[6] with applied stress. These considerations apply, of course, to either form of the $5d^9$ dihedral model indicated in Fig. 5. In addition, the very small value $2\Delta_{rh}=4.4$ meV for the crystal-field splitting of the α and β $5d$ orbitals in the distorted configuration proposed by Ammerlaan and van Oosten would contrast to the strong coupling found for the $5d$ orbitals of Pt-group transition metals in other hosts.[40]

V. DISCUSSION

The fact that the vacancy model for Pt^- yields the same JT-distorted symmetry (C_{2v}) and spin ($S=\frac{1}{2}$) as for V^-, as observed experimentally, represented the initial success for Watkins's proposal[9] of this model. At first sight surprising, therefore, is the finding in paper I (Ref. 6) that the experimental strain-coupling coefficients of Pt^- (Table III) have the opposite sign from those of V^-, indicating the opposite sense of the JT distortions for these defects in both tetragonal and trigonal modes. As we have seen, however, in the t_2^3 configuration the JT stabilization energy in the vacancy model is the same for either sense of the distortion as long as only linear coupling is considered, and the form of the distortion that occurs must therefore be determined by nonlinear coupling that has the opposite effect for the two defects. When the sense of each distortion is recognized, the signs of the one-electron strain-coupling coefficients (Table IV) turn out to be the same for Pt^- as for V^-, as expected if the vacancy model holds, though the presence of the impurity at the substitutional site evidently affects the magnitude of these coefficients. The vacancy model for Pt^- is thus entirely successful in accounting qualitatively for the form of the spontaneous JT distortion and the defect's response to an applied stress, on the basis of the known behavior of V^-.

The detailed development of the vacancy model that we have described also accounts very satisfactorily for the unusual features of the EPR spectrum of Pt^- as reported originally by Woodbury and Ludwig,[1] in particular the approximately axial form of the g tensor with respect to a $\langle 001 \rangle$ axis and its large departure from a spin-only value 2. That $g_{zz}=g_\parallel$ is significantly greater than 2 is the result, according to Eq. (18), of a contribu-

tion to the orbital g factor from the $t_2(5d)$ orbitals of the central Pt, although this admixture into the t_2 manifold is found to be only of order 10%, quite consistent with the predominant vacancylike character of these orbitals postulated in the vacancy model. The even larger reduction in $g_\perp = \frac{1}{2}(g_{xx}+g_{yy})$ to a value substantially smaller than 2 occurs not because of an orbital contribution to $g_\perp$ but, again according to Eq. (18), because spin-orbit interaction from the Pt $5d$ shell is comparable with the splitting of the α and β orbitals by the trigonal component of the distorted crystal field and thereby reduces the spin contribution to $g_\perp$. The small departure $g_{xx}-g_{yy}$ from axial symmetry, given by Eq. (67), should be attributable only to the residual spin-orbit coupling of these orbitals to the more distant state $|\zeta\rangle$, which is split off by the tetragonal component of the crystal field. Only this small anisotropy $g_{xx}-g_{yy}$ fails to fit in detail to our analysis of the vacancy model, presumably as shown elsewhere by Anderson *et al.*[14] because a precise numerical fit requires coupling to other states outside the t_2 manifold that for simplicity we have omitted. The vacancy model also describes very satisfactorily the observed hyperfine coupling with the Pt and its anisotropy in particular. The contact hyperfine coupling obtained for the Pt presumably is the result in large part of exchange polarization of filled states in the valence band and should not be taken as evidence of localization of the gap orbitals. Finally, the vacancy model explains satisfactorily why superhyperfine coupling is observed with but two of the four nearest-neighbor Si atoms.

The alternative $5d^9$ dihedral model of Ammerlaan and van Oosten,[8] by contrast, permits an exact fit of the g tensor, including its anisotropy, but fails to describe the Pt hyperfine anisotropy $A_{xx}-A_{yy}$ for any reasonable values for the two parameters A_c and PN^2. Also, as we have seen in Sec. IV, it fails to ensure that the superhyperfine coupling is with only two of the neighboring Si atoms. As shown by Ammerlaan and van Oosten, this model requires taking $N^2=0.73$, a degree of localization of the t_2 orbital in the Pt $5d$ shell that supports their conclusion that their model is not compatible with the vacancy model. As we have also shown in Sec. IV, a clear experimental test for their model lies in determining experimentally the sign of the product $g_{xx}g_{yy}g_{zz}$, which Ammerlaan and van Oosten took to be negative and which the vacancy model predicts is positive.

We have shown that the $5d^9$ dihedral model admits a second solution, not considered by Ammerlaan and van Oosten, which gives a precise fit to the g tensor of Pt$^-$ with only $\sim 7\%$ localization in the Pt $5d$ orbitals. This solution yields a positive value for $g_{xx}g_{yy}g_{zz}$ and locates the wave function on the correct pair of neighboring Si atoms. But this model, like that of Ammerlaan and van Oosten, fails to describe the anisotropy in the Pt hyperfine coupling and does not yield the correct form of JT distortion. The model for Pt$^-$ proposed in 1980 by Lowther[7] to fit the g tensor apparently corresponds to this alternative form of the $5d^9$ dihedral model, although fitting the data to this model requires that the sign of $g_\perp$ be the opposite of that given by Lowther.

It has been found in paper I that the Pt$^-$ defect reorients effectively instantaneously upon the application or removal of stress, even at ~ 2 K, and thus immediately re-establishes an equilibrium distribution among its six possible orientations. We take this ease of reorientation not only as evidence that the distortion from tetrahedral symmetry is spontaneous via the JT effect but as an indication that the JT distortion, though evidently "static" in form at low temperatures, is close to revealing a dynamic behavior of vibronic origin, such as tunneling between different distorted configurations. In this connection it may be noted, from Eq. (60) and the value $\cos 2\theta \cong 0.7$ inferred from Sec. III A, that an increase of less than 50% in the spin-orbit coupling (or a corresponding decrease in V_T^2/k_T) should suffice to eliminate the instability associated with the trigonal distortion mode, according to the inequality (59). In any case, it appears that the trigonal distortion, which involves the displacement of the Pt atom along the axis of tetragonal distortion, cannot be large, since otherwise the heavy Pt mass should eliminate the possibility of tunneling and thus require thermal activation over a significant barrier such as that given by $(E_{\rm JT})_{\rm trig}$ in Eq. (61) in order that reorientation occurs. We speculate that this heavy Pt mass stabilizes the static JT distortion but still allows rapid reorientation via some vibronic process. Supporting the vibronic nature of the Pt$^-$ defect is the unusual observation reported in paper I of an isotope shift in the g tensor, which depends on the isotopic composition of the Si nearest neighbors. A further analysis of aspects of the vacancy model that could account for such an effect will be described in a later paper.

A curious feature of our calculation of the g tensor is that the crystal-field splitting of the doublet $|\xi\rangle$, $|\eta\rangle$ due to the trigonal distortion can be large with respect to the spin-orbit splitting, yet the g tensor will remain nearly axial with respect to the tetragonal axis so long as the singlet $|\zeta\rangle$ is separated from the doublet by an energy large enough that spin-orbit coupling to $|\zeta\rangle$ is small. Yet the perpendicular component $g_{xx}\cong g_{yy}\cong g_\perp$ is not approximately zero, as it would be according to Eqs. (8)–(11) if the symmetry were truly tetragonal, but according to Eq. (18) can be anywhere in the range $0<|g_\perp|<g_e$. This behavior is clearly shown by our development of the vacancy model and of the alternative form of the $5d^9$ dihedral model and is implicit in the analysis given by Bleaney and O'Brien.[22] (Taking $\sin\alpha=0$ in their work, one finds $g_x=-g_y$ in the axial case for their choice of the effective spin.) Their work also shows that the possibility of a nearly axial g tensor is not limited to any particular symmetry for the defect, so long as one of the t_2 levels is well separated from the other two.

ACKNOWLEDGMENTS

One of us (F.G.A.) would like to acknowledge his gratitude to the Max-Planck-Institute (Stuttgart) for their hospitality and support during the time in which the theoretical ideas reported in this paper came to fruition. The contributions of F.S.H. to this research were supported

by the U.S. Office of Navel Research (Electronics and Solid State Program) under Contract No. N00014-90-J-1264. We would like to thank C. A. J. Ammerlaan and A. B. van Oosten for making available copies of their work prior to publication.

APPENDIX: PROPERTIES OF THE KRAMERS DOUBLET (L,L^*)

The Kramers doublet complementary to (H,H^*) at the lower energy as given by Eq. (17) is given by

$$|L\rangle = -\sin\theta|A'\rangle + \cos\theta|B\rangle ,$$
$$|L^*\rangle = -\sin\theta|A'^*\rangle + \cos\theta|B^*\rangle , \tag{A1}$$

with θ given by Eq. (16). Its g tensor in the axial approximation ($\cos\alpha = 1$) corresponding to Eq. (18) is

$$g_{zz} = g_e + 2g_{\mathcal{L}}\cos 2\theta ,$$
$$g_{\perp} = -g_e \sin 2\theta . \tag{A2}$$

Representing (L,L^*) exactly within the t_2 gap manifold, we may use an expression identical with that for (H,H^*) in Eq. (21) in terms of coefficients u,v,w, except that these coefficients are now given from Eqs. (12) and (A1) by

$$u = -\sin\theta\cos\alpha ,$$
$$v = \cos\theta , \tag{A3}$$
$$w = \sin\theta\sin\alpha ,$$

in terms of α and θ from Eqs. (13) and (16). The exact g tensor is then given by the same expression used for (H,H^*) in Eq. (25), except that the coefficients u,v,w are now to be taken from Eq. (A3). A similar procedure yields the Pt hyperfine tensor for (L,L^*) by substituting from Eq. (A3) into Eqs. (32)–(34). The ^{29}Si hyperfine tensors are as given by Eq. (41) except that p_α^H and p_β^H are to be replaced for (L,L^*) (for $\cos\alpha \cong 1$) by

$$p_\alpha^L = \tfrac{1}{2}(u+v)^2 = \tfrac{1}{2}(\cos\theta - \sin\theta)^2$$
$$p_\beta^L = \tfrac{1}{2}(u-v)^2 = \tfrac{1}{2}(\cos\theta + \sin\theta)^2 . \tag{A4}$$

Comparing Eq. (42) with Eq. (A4), we note that if (H,H^*) has $p_\alpha^H > p_\beta^H$ so that the ^{29}Si hyperfine coupling is predominantly on sites a and d, (L,L^*) has $p_\alpha^L < p_\beta^L$, and the coupling is predominantly on b and c as expected, and vice versa.

These expressions for (L,L^*) are appropriate to both the vacancy model and to the $5d^9$ dihedral model considered by Ammerlaan and van Oosten (Sec. IV). In the latter case, however, one has $\lambda > 0$, so that α as given still by Eq. (13) is positive when the doublet states $|\alpha\rangle$ and $|\beta\rangle$ are below $|\zeta\rangle$ ($\Delta_\zeta > 0$) as on the right-hand side of Fig. 5. With $\lambda > 0$, θ as given by Eq. (16) now is to be taken in the range $\pi/4 < \theta < \pi/2$ for $V_T Q_\zeta < 0$ and $-\pi/2 < \theta < -\pi/4$ for $V_T Q_\zeta > 0$. This choice of θ for $\lambda > 0$, together with that given for $\lambda < 0$ in Sec. II B, insures that the Kramers doublet (H,H^*) given by Eq. (15) always lies at a higher energy than (L,L^*), given by Eq. (A1).

[1] H. H. Woodbury and G. W. Ludwig, Phys. Rev. **126**, 466 (1962).
[2] J. C. M. Henning and E. C. J. Egelmeers, Phys. Rev. B **27**, 4002 (1983).
[3] R. F. Milligan, F. G. Anderson, and G. D. Watkins, Phys. Rev. B **29**, 2819 (1984).
[4] P. Omling, P. Emanuelson, and H. G. Grimmeiss, Phys. Rev. B **36**, 6202 (1987).
[5] A. B. van Oosten, N. T. Son, L. S. Vlasenko, and C. A. J. Ammerlaan, in *Defects in Semiconductors XV,* edited by G. Ferenczi (Trans Tech, Aedermannsdorf, 1989), p. 355.
[6] F. G. Anderson, R. F. Milligan, and G. D. Watkins, preceding paper, Phys. Rev. B **45**, 3279 (1992).
[7] J. E. Lowther, J. Phys. C **13**, 3681 (1980).
[8] C. A. J. Ammerlaan and A. B. van Oosten, Phys. Scr. **T25**, 342 (1989).
[9] G. D. Watkins, Physica B **117&118**, 9 (1983).
[10] B. G. Cartling, J. Phys. C **8**, 3183 (1975).
[11] L. A. Hemstreet, Phys. Rev. B **15**, 834 (1977).
[12] A. Zunger and V. Lindefelt, Phys. Rev. B **27**, 1191 (1983).
[13] G. D. Watkins, in *Deep Centers in Semiconductors,* edited by S. T. Pantelides (Gordon and Breach, New York, 1986), p. 147.
[14] F. G. Anderson, C. Delerue, M. Lannoo, and G. Allan, Phys. Rev. B **44**, 10 925 (1991).
[15] J. L. A. Alves and J. R. Leite, Phys. Rev. B **30**, 7284 (1984).
[16] M. Lannoo, Phys. Rev. B **36**, 9355 (1987).
[17] A. Abragam and M. H. L. Pryce, Proc. R. Soc. London Ser. A **205**, 135 (1951).
[18] The ground-state ($5d^9\,^2D$) spin-orbit splitting of Pt II is taken as an approximation to $-(5/2)\zeta_{\mathrm{Pt}}$ [C. E. Moore, *Atomic Energy Levels,* Natl. Bur. Stand. (U.S.) Circ. No. 467 (U.S. GPO, Washington, D. C., 1958), Vol. III, pp. 183–185].
[19] Hyperfine interaction with ^{29}Si (Sec. III A) shows that dangling bonds at nearest-neighbor sites are tilted away from $\langle 111\rangle$ crystal directions and make an angle of $\pm 10.4°$ with the x axis of the defect. Such a tilting of the bond could lead to a contribution to the orbital g factor $g_{\mathcal{L}}$ from the part of the wave function on the silicon neighbors. We omit the possibility of such a contribution in the model considered in this paper, taking $g_{\mathcal{L}}$ as in Eq. (7) to be approximated by the contribution of the central Pt.
[20] A. Abragam and B. Bleaney, *Electron Paramagnetic Resonance of Transition Ions* (Clarendon, Oxford, 1970), Chap. 3, p. 133.
[21] G. F. Koster, J. O. Dimmock, R. G. Wheeler, and H. Statz, *Properties of the Thirty-Two Point Groups* (MIT, Cambridge, MA, 1963), p. 36.
[22] B. Bleaney and M. C. M. O'Brien, Proc. Phys. Soc. London Sect. B **69**, 1216 (1956).
[23] A. Abragam and B. Bleaney, *Electron Paramagnetic Resonance of Transition Ions* (Ref. 20), p. 690.
[24] A. K. Koh and D. J. Miller, At. Data Nucl. Data Tables **33**, 235 (1985).
[25] A. Abragam and B. Bleaney, *Electron Paramagnetic Resonance of Transition Ions* (Ref. 20), p. 702.

[26]F. S. Ham, Phys. Rev. **138**, A1727 (1965); F. S. Ham, W. M. Schwarz, and M. C. M. O'Brien, *ibid.* **185**, 548 (1969).

[27]G. D. Watkins and J. W. Corbett, Phys. Rev. **134**, A1359 (1964), Table III.

[28]A. A. Kaplyanskii, Opt. Spektrosk. **16**, 602 (1964) [Opt. Spectrosc. (USSR) **16**, 329 (1964)].

[29]F. S. Ham, in *Electron Paramagnetic Resonance,* edited by S. Geschwind (Plenum, New York, 1972), p. 1.

[30]M. D. Sturge, in *Solid State Physics,* edited by F. Seitz, D. Turnbull, and H. Ehrenreich (Academic, New York, 1967), Vol. 20, p. 91.

[31]F. S. Ham, Phys. Rev. **166**, 307 (1968).

[32]Anderson *et al.* (Ref. 14) have shown that it is possible to fit $A_{xx}-A_{yy}$ and the g factors, including the correct anisotropy $g_{xx}-g_{yy}=-0.04$, by augmenting the three parameters $g_{\perp}$, θ, and w [with values roughly approximating those in Eq. (63) and the last row of Table II] by a phenomenological parameter representing the coupling of the state $|\zeta\rangle$ in Eq. (21) with the Pt orbital $|E\theta\rangle$ through the trigonal distortion. Additional coupling of the Kramers doublet (H,H^*) to both d orbitals $|E\theta\rangle$ and $|E\epsilon\rangle$ may also occur through spin-orbit interaction.

[33]E. Simanek, K. Sroubek, K. Zdansky, J. Kaczer, and L. Novak, Phys. Status Solidi **14**, 333 (1966).

[34]A. J. Freeman, J. V. Mallow, and P. S. Bagus, J. Appl. Phys. **41**, 1321 (1970).

[35]H. Katayama-Yoshida and K. Shindo, Phys. Rev. Lett. **51**, 207 (1983).

[36]A. Zunger, in *Solid State Physics,* edited by H. Ehrenreich and D. Turnbull (Academic, New York, 1986), Vol. 39, p. 275.

[37]G. A. Baraff, E. O. Kane, and M. Schlüter, Phys. Rev. Lett. **43**, 956 (1979); Phys. Rev. B **22**, 5662 (1980).

[38]A. Hjortsberg, J. T. Vallin, and F. S. Ham, Phys. Rev. B **37**, 3196 (1988).

[39]M. H. L. Pryce, Phys. Rev. Lett. **3**, 375 (1959); A. Abragam and B. Bleaney, *Electron Paramagnetic Resonance of Transition Ions* (Ref. 20), p. 139.

[40]J. H. E. Griffiths, J. Owen, and I. M. Ward, Proc. R. Soc. London Ser. A **219**, 526 (1953).